

1 **MARK2/MARK3 kinases are catalytic co-dependencies of YAP/TAZ in human**
2 **cancer**

3

4 Olaf Klingbeil¹, Damianos Skopelitis¹, Claudia Tonelli¹, Aktan Alpsoy¹, Francesca Minicozzi¹, Disha
5 Aggarwal^{1,2}, Suzanne Russo¹, Taehoon Ha¹, Osama E. Demerdash¹, David L. Spector^{1,2}, David A.
6 Tuveson^{1,3}, Paolo Cifani¹, and Christopher R. Vakoc^{1,4*}

7

8 **Affiliations:**

9 ¹Cold Spring Harbor Laboratory, Cold Spring Harbor, New York, 11724, U.S.A.

10 ²Graduate Program in Genetics, Stony Brook University, Stony Brook, New York 11794

11 ³Lustgarten Foundation Pancreatic Cancer Research Laboratory, Cold Spring Harbor, NY 11724, USA

12 ⁴Lead contact

13 *Correspondence: vakoc@cshl.edu

14 **Abstract**

15 The Hippo signaling pathway is commonly dysregulated in human cancer, which leads to a powerful
16 tumor dependency on the YAP/TAZ transcriptional coactivators. Here, we used paralog co-targeting
17 CRISPR screens to identify the kinases MARK2/3 as absolute catalytic requirements for YAP/TAZ
18 function in diverse carcinoma and sarcoma contexts. Underlying this observation is direct MARK2/3-
19 dependent phosphorylation of NF2 and YAP/TAZ, which effectively reverses the tumor suppressive
20 activity of the Hippo module kinases LATS1/2. To simulate targeting of MARK2/3, we adapted the
21 CagA protein from *H. pylori* as a catalytic inhibitor of MARK2/3, which we show exerts anti-tumor
22 activity *in vivo*. Together, these findings reveal MARK2/3 as powerful co-dependencies of YAP/TAZ
23 in human cancer; targets that may allow for pharmacology that restores Hippo pathway-mediated tumor
24 suppression.

25 **Introduction**

26 The Hippo signaling pathway is a conserved regulator of cell identity and proliferation during metazoan
27 development, with additional roles in tissue regeneration and in cancer progression (3). In mammals, the
28 core of the Hippo pathway includes the kinases LATS1/2, which catalyze inhibitory phosphorylation of
29 the YAP/TAZ transcriptional coactivators (4,5). LATS1/2 activity is, in turn, activated by MST1/2 and
30 MAP4K kinases and by the scaffolding protein NF2, which are themselves regulated by signals from the
31 tissue microenvironment (6-11). Once released from LATS1/2-mediated inhibition, YAP/TAZ can enter
32 the nucleus and bind to TEAD transcription factors to activate a transcriptional program of cell
33 proliferation and lineage plasticity (12-14).

34

35 YAP/TAZ and its upstream Hippo pathway are commonly dysregulated in human carcinomas and
36 sarcomas to promote tumor development (1,2). This can occur via genetic (e.g. *YAP/TAZ*
37 amplifications)(1) or non-genetic (e.g. perturbations of the extracellular matrix, metabolism, or cell
38 polarity)⁽¹⁵⁻¹⁹⁾ mechanisms, with a consequence being that many human cancers possess a powerful
39 dependency on the function of YAP/TAZ to sustain tumor growth. Since YAP/TAZ activity is
40 dispensable for the homeostasis of several tissues (20-22), the aberrant functioning of this pathway has
41 motivated efforts to develop drugs that interfere with YAP/TAZ function, such as small molecules that
42 block the interaction between YAP/TAZ and TEAD proteins (23-26). However, a major obstacle in this
43 effort has been in identifying ‘druggable’ targets that allow for the restoration of Hippo-mediated tumor
44 suppression in YAP/TAZ-dependent cancers.

45 **Results**

46 Paralog co-targeting CRISPR screens identify MARK2/3 as context-specific cancer dependencies

47 Here, we developed a dual sgRNA CRISPR vector system for performing double knockout screens of
48 gene paralogs in search of redundant cancer cell dependencies (Fig. 1a). Using this system, we cloned a
49 pooled library of 64,697 dual guide RNAs designed to generate 1,719 single gene knockouts and 2,529
50 paralog double knockouts, focusing on factors involved in signal transduction and epigenetic regulation
51 (Fig. 1a, Supplementary Table 1,2). For each gene, we designed sgRNAs targeting exons that encode
52 conserved protein domains to maximize the efficiency of generating loss-of-function alleles (27). We
53 used this library to perform negative-selection screens in 22 cancer cell lines grown under standard 2D
54 culture conditions, which represent a diverse set of tumor lineages and genotypes (Supplementary Table
55 3). The performance of control sgRNAs within this library supported the accuracy of these screening
56 datasets (Supplementary Fig. S1a). For each double knockout, we quantified the degree of genetic
57 redundancy using the GEMINI algorithm (28), which validated paralogs that are known to support
58 cancer growth in a redundant manner, such as *HDAC1/HDAC2*, *ESCO1/ESCO2*, and *EP300/CREBBP*
59 (Fig. 1b, Supplementary Table 4-6) (29-31). By excluding pan-essential paralog pairs required for all
60 cancer cell lines tested, we nominated the kinase paralogs *MARK2* and *MARK3* as outliers showing both
61 robust redundancy and cell line selectivity as cancer dependencies (Fig. 1b, Supplementary Fig. S1b).
62 While prior studies have identified functions for specific MARK kinases in cancer (32-34), the essential
63 redundant function of MARK2/3 in human cancer cells has, to our knowledge, not been previously
64 defined.

65

66 To validate these screening results, we performed arrayed-format competition-based proliferation
67 experiments in a panel of 31 cancer cell lines (Fig. 1c, 1d, Supplementary Fig. S1c, Supplementary Table
68 3). These assays validated the redundancy and essentiality of MARK2/3 in 19 cancer lines, whereas 12

69 cancer lines proliferated normally despite effective MARK2/3 double knockout, confirmed by western
70 blotting (Fig. 1e, Supplementary Fig. S1d). In these experiments, we noticed that MARK2/3 dependency
71 was biased towards carcinomas and sarcomas, whereas most hematopoietic and neuroendocrine lineage
72 cancers proliferated independently of MARK2/3 (Fig. 1c). Knockout of MARK2/3 led to a G0/G1 cell
73 cycle arrest and apoptosis in pancreatic (YAPC) and breast (MDA-MB231) adenocarcinoma lines, with
74 a potency that resembled the effects of inactivating the mutant *KRAS* oncogene present in these models
75 (Fig. 1f, 1g, Supplementary Fig. S1e-g). MARK2/3 knockout in YAPC xenografts led to robust tumor
76 growth inhibition *in vivo* (Supplementary Fig. S1h, 1i). Expression of a CRISPR-resistant *MARK2* or
77 *MARK3* cDNA alleviated the cell fitness defect caused by the double knockout, indicating on-target
78 effects (Fig. 1h, Supplementary Fig. S1k). Using this cDNA rescue assay, we found that mutational
79 inactivation of kinase activity (*MARK2*^{K82H}) compromised cancer cell proliferation (Supplementary Fig.
80 S1j, 1l). We further validated the importance of MARK2/3 catalytic function using a bump-and-hole
81 strategy(35), in which replacement of endogenous MARK2/3 with *MARK2*^{M129G}, rendered the
82 proliferation of YAPC cells sensitive to the bulky kinase inhibitor 1NM-PP1 (Fig 1i and Supplementary
83 Fig. S1j, 1l). Collectively, these experiments validated MARK2/3 as catalytic dependencies in specific
84 carcinoma and sarcoma cell line models.

85

86 MARK2/3 dependency in cancer is linked to the maintenance of YAP/TAZ function

87 We next sought to understand why MARK2/3 is essential in some cancer contexts, but dispensable in
88 others. Using comparative transcriptome analysis, we found that the MARK2/3 essentiality across the
89 31 cancer lines was highly correlated with the expression of *YAP* and *TAZ* and with the expression of
90 canonical YAP/TAZ target genes *MYOF*, *CYR61*, *DKK1*, and *CAVI* (Fig. 2a, 2b) (36-38). Using dual
91 sgRNA vectors, we confirmed that YAP and TAZ function redundantly as dependencies in this cell line
92 panel in a manner that closely correlated with MARK2/3 essentiality (Fig. 2b, 2c Supplementary Fig.

93 S2a, 2b). This observation led us to hypothesize that MARK2/3 is critical for maintaining YAP/TAZ
94 function in diverse human cancer contexts. In support of this, we found that the inactivation of MARK2/3
95 led to reduced expression of a fluorescence-based TEAD:YAP/TAZ reporter in MDA-MB231 cells (Fig.
96 2d) (18). In addition, RNA-seq analysis performed in 20 different cancer cell line models following
97 MARK2/3 knockout demonstrated reduced expression of a YAP/TAZ transcriptional signature in
98 MARK2/3-dependent lines (Fig. 2e-g, Supplementary Table 7). We extended this analysis by performing
99 genome-wide profiling of active chromatin (H3K27 acetylation), which revealed that MARK2/3 and
100 YAP/TAZ are each critical to activate a shared set of TEAD4:YAP-bound enhancer elements (Fig. 2h,
101 2i, Supplementary Fig. S2c-e). Together, these results suggest that MARK2/3 are required to maintain
102 the essential function of YAP/TAZ in human cancer.

103

104 MARK2/3 catalyze inhibitory phosphorylation of NF2 and activating phosphorylation of YAP/TAZ

105 Upon inactivating MARK2/3, we observed a striking increase in LATS1/2 T1079/T1041
106 phosphorylation (Fig 3a, 3b, Supplementary Fig. S3a). This activation mark is known to be catalyzed
107 redundantly by MST1/2 and MAP4K kinases, whose activity is further enhanced by NF2 (Fig. 3a) (6).
108 Knockout of MARK2/3 triggered reduced nuclear levels of YAP/TAZ, which is an expected outcome
109 of strengthening LATS1/2 function (Fig. 3c). While prior studies have shown that MARK2/3 inhibits
110 the function of MST1/2 (34,39,40), we reasoned that this substrate would be insufficient to account for
111 the MARK2/3 dependency in cancer, since MST1/2 function redundantly with MAP4Ks to regulate
112 YAP/TAZ in human cells (see below)^(6,8). This prompted us to perform a broader exploration of
113 MARK2/3 substrates in the Hippo pathway using a chemical-genetic strategy (Fig. 3d) (41). Our
114 approach exploited gatekeeper substitutions of MARK2 (M129G) and MARK3 (M132G), which can
115 accommodate bulky ATP- γ -S analogs (e.g. 6-Fu-ATP- γ -S). We co-expressed MARK2^{M129G} or
116 MARK3^{M132G} with 18 different epitope-tagged Hippo pathway components in HEK293T cells, followed

117 by treatment with 6-Fu-ATP- γ -S and immunoprecipitation-western blotting with a phospho-thio-ester-
118 specific antibody. This approach validated the known ability of MARK2/3 to phosphorylate CDC25C
119 and MST1/2, in accord with prior findings (Supplementary Fig. S3b-d) (34,42). In addition, we identified
120 NF2, YAP, and, to a lesser extent, TAZ, as MARK2/3 substrates in this system (Supplementary Fig.
121 S3b-d). Importantly, we did not detect MARK2/3-dependent phosphorylation of LATS1/2, but we
122 detected robust phosphorylation of several MAP4K kinases (Supplementary Fig. S3b-d). To map the
123 exact sites of phosphorylation, we performed *in vitro* kinase assays with purified MARK2 and each
124 substrate, followed by mass spectrometric peptide quantification (Supplementary Fig. S3e-g). In these
125 assays, MARK2 catalyzed phosphorylation on serine or threonine residues of NF2 (4 sites), YAP (5
126 sites), and TAZ (4 sites) (Fig. 3e-g, Supplementary Fig. S4a-k, Supplementary Table 8). By introducing
127 alanine substitutions of these phosphosites into cDNA constructs, we confirmed the importance of these
128 specific serine/threonine residues for MARK2-dependent phosphorylation in human cells
129 (Supplementary Fig. S5a-e). Using mass spectrometry analysis, we also identified sites of MARK2-
130 dependent phosphorylation on MAP4K proteins and MST1/2 (Supplementary Fig. S3g), however the
131 known redundancy among these kinases (6) led us to prioritize NF2 and YAP/TAZ for further functional
132 investigation (Fig. 3a).

133

134 Two of the sites of MARK2/3-dependent phosphorylation on NF2 were T230 and S315, which have
135 been reported to inhibit NF2 function (43). To further evaluate this, we used a transfection-based assay
136 in HEK293T cells (6,44), in which NF2 overexpression stimulates p-LATS1/2. We found that co-
137 expression of wild-type MARK2/3, but not a catalytically dead mutant, negated NF2-stimulated
138 LATS1/2 phosphorylation (Fig. 3h, Supplementary Fig. S5f). In addition, a phospho-mimetic allele of
139 NF2, in which all four sites of MARK2-dependent phosphorylation are substituted with aspartate, was
140 incapable of triggering LATS1/2 phosphorylation (Fig. 3i, Supplementary Fig. S5g). We also found that

141 MARK2 was able to disrupt the physical interaction between NF2 and MAP4K kinases and block
142 MAP4K4/6-dependent LATS1 phosphorylation (Supplementary Fig. S5h-k) (6). Knockout of
143 MARK2/3 triggered increased levels of JUN phosphorylation, a known downstream target of MAP4K
144 kinases (Supplementary Fig. S5l, 5m) (45). Together, our findings suggest that MARK2/3 can indirectly
145 suppress LATS1/2 activity by directly phosphorylating upstream components of the Hippo pathway.

146

147 We next evaluated the functional importance of YAP/TAZ phosphorylation by MARK2/3. LATS1/2
148 have been shown to sequester YAP/TAZ in the cytoplasm by installing phosphorylation that is
149 recognized by 14-3-3 proteins (46). Owing to the adjacent locations of several MARK2/3 and LATS1/2
150 substrates on YAP/TAZ (Fig. 3f, 3g) (47,48), we hypothesized that MARK2/3-dependent
151 phosphorylation might release YAP/TAZ from 14-3-3-mediated inhibition. To evaluate this, we
152 reconstituted LATS1/2-dependent YAP/TAZ phosphorylation using purified proteins (Fig. 3j,
153 Supplementary Fig. S5n), which was sufficient to trigger interactions with recombinant 14-3-3 ϵ (Fig.
154 3k, 3l). However, pre-incubation of recombinant YAP or TAZ with MARK2 or MARK3 and ATP
155 eliminated the formation of 14-3-3 ϵ complexes despite the presence of LATS1/2-dependent
156 phosphorylation (Fig. 3k, 3l). In accord with these *in vitro* findings, expression of a phospho-mimetic
157 allele of YAP or TAZ, in which all MARK2/3 substrates are mutated to aspartic acid, eliminated the 14-
158 3-3 ϵ interaction in cellular lysates (Fig. 3m, 3n). Collectively, these functional experiments support that
159 MARK2/3-dependent phosphorylation of YAP/TAZ can disrupt the LATS1/2-dependent formation of
160 14-3-3 complexes.

161

162 Regulation of NF2 and YAP accounts for the essential functions of MARK2/3 in human cancer

163 The biochemical findings above prompted us to perform epistasis experiments evaluating whether dual
164 regulation of NF2 and YAP/TAZ underlies the essential function of MARK2/3 in cancer identified in
165 our paralog screen. As expected, we found that the pharmacological inhibition or double knockout of
166 MST1/2, or its adaptor SAV1, failed to alleviate the MARK2/3 dependency (Fig. 4a, 4b, Supplementary
167 Fig. S6a-d). In contrast, inhibition or double knockout of LATS1/2 resulted in a bypass of MARK2/3
168 essentiality in four different cancer cell line models (Fig. 4a, 4c, Supplementary Fig. S6c,d). In these
169 same models, we found that NF2 knockout or expression of a phosphomimic allele of YAP (YAP^{5D})
170 partially alleviated the MARK2/3 dependency (Fig. 4d, 4e, Supplementary Fig. S6e). Moreover,
171 combining the NF2^{KO}/YAP^{5D} genetic alterations led to a nearly complete bypass of MARK2/3
172 dependency in these contexts, which resembles the effects of inactivating LATS1/2 (Fig. 4a, 4e).
173 Collectively, these results suggest that an essential function of MARK2/3 in cancer is to regulate NF2
174 and YAP/TAZ, which allows for potent indirect control over the output of LATS1/2.

175

176 Inducible expression of a protein-based MARK2/3 inhibitor re-instates Hippo-mediated tumor
177 suppression in organoid and xenograft tumor models

178 The Hippo pathway activity is known to be modulated by cell culture conditions (18), which motivated
179 us to validate MARK2/3 dependency in tumor models with more physiological extracellular
180 environments. Since selective small-molecule inhibitors of MARK kinases are not available, we
181 developed a catalytic inhibitor of MARK kinase activity that could be expressed in an inducible manner
182 in various tumor models. The EPIYA repeat region of the CagA protein of *H. pylori* was reported to
183 potently and selectively inhibit MARK kinase activity by competing with substrate binding (49,50), a
184 peptide we refer to here as MARK kinase inhibitor (MKI) (Fig. 5a). We observed that lentiviral
185 expression of MKI, but not an MKI peptide harboring point mutations that abrogate MARK binding
186 (50), reduced the nuclear levels of YAP/TAZ and suppressed the expression of a YAP/TAZ

187 transcriptional signature (Fig 5b-e, Supplementary Fig. S7a). In addition, the proliferation arrest induced
188 by MKI correlated with the overall sensitivity to MARK2/3 double knockout in a cell line panel (Fig.
189 5c). Our epistasis experiments further indicated that engineering of NF2^{KO}/YAP^{5D} alleviated the
190 sensitivity to MKI-mediated growth (Fig. 5f), thus validating MKI as a tool catalytic inhibitor that
191 mimics the biological effects of MARK2/3 double knockout when expressed in cancer cells.

192

193 We next engineered a vector that expresses MKI under the control of a doxycycline-inducible promoter,
194 which was introduced into a panel of *YAP*- or *TAZ*-amplified human triple-negative breast cancer or
195 pancreatic ductal adenocarcinoma organoid cultures. Dox-inducible expression of MKI in these models
196 led to a strong reduction of cancer cell viability (Fig. 5g). We also introduced the dox-inducible MKI
197 (wild-type versus mutant) expression constructs into pancreatic adenocarcinoma cells (YAPC), which
198 were transplanted subcutaneously into immune-deficient mice. After the tumors were established (day
199 10), we administered doxycycline and observed that MKI, but not the point mutant control, led to a
200 potent reduction of tumor growth *in vivo* (Fig. 5h Supplementary Fig. S7b,c). The findings validate the
201 potent anti-tumor effects of catalytic MARK2/3 inhibition in YAP/TAZ-dependent cancers.

202

203 **Discussion**

204 It has been observed that human cancers can be broadly classified based on the status of YAP/TAZ(51).
205 YAP/TAZ^{OFF} tumors tend to be of hematopoietic or neural/neuroendocrine lineages, and in this context
206 transcriptional silencing of YAP/TAZ is required for tumor development (51-53). In contrast, YAP/TAZ
207 are activated in human carcinomas and sarcomas, which is essential for tumorigenesis (51,54). This
208 binary classification has important clinical implications, as YAP/TAZ have powerful effects on several
209 tumor cell phenotypes, including epigenetic plasticity and drug sensitivities (2,55). Here, we have

210 exploited the ON vs OFF status of this pathway to reveal a strict requirement for MARK2/3 catalytic
211 activity to support YAP/TAZ function across a diverse array of human carcinomas and sarcomas.
212 Targeting of MARK2/3 leads to potent inhibition of YAP/TAZ and a severe compromise of tumor cell
213 fitness; phenotypes that can be accounted for by phosphorylation of NF2 and YAP as direct MARK2/3
214 substrates. Our study positions MARK2/3 as dominant regulators of the human Hippo pathway, and
215 hence a ‘druggable’ target in YAP/TAZ-dependent tumors.

216

217 Early genetic studies in model organisms implicated the MARK1-4 ortholog Par-1 as key regulator of
218 cell polarity (56,57). Importantly, work in *Drosophila* identified Par-1 as a negative regulator of the
219 Hippo pathway, which influences cell growth phenotypes in this organism (39). Despite this early
220 observation, the connection between MARKs and Hippo in human cells has been controversial, with
221 some studies suggesting MARKs can activate (34,39,40) or inhibit (33,58) YAP/TAZ function. Since
222 these prior studies focused on the genetic manipulation of individual MARK kinase genes, genetic
223 redundancy between MARK2/3 likely concealed the powerful inhibitory influence of human MARK
224 kinases over the Hippo pathway. While our findings are generally consistent with the earlier *Drosophila*
225 study(39), the mechanism by which MARK/Par-1 regulate YAP/TAZ appears to be distinct in each
226 organism, with an expansion of upstream and downstream substrates of MARK2/3 in human cells that
227 allow for multi-level control over the output of LATS1/2. Nevertheless, this work suggests an ancient
228 linkage between MARK and Hippo during metazoan evolution, which may have emerged to integrate
229 cellular polarity with organ growth and regeneration.

230

231 Prior studies have described small-molecules that block the interaction between YAP/TAZ and TEAD
232 transcription factors (23-26,59), which are currently the most developed therapeutic strategy for
233 targeting Hippo-dysregulated cancers (60). While the efficacy of such an approach in human patients

234 has only recently begun to be evaluated in clinical trials (61,62), our work reveals chemical inhibition of
235 MARK2/3 kinase activity as an alternative strategy for eliminating YAP/TAZ-addicted tumor cells. As
236 kinases, chemical inhibition of MARK2/3 could achieve desirable selectivity and potency by leveraging
237 decades of experience in the pharmaceutical industry at targeting this class of enzymes (63), which would
238 differ from the challenges of modulating a protein-protein interaction (64,65). In addition, by functioning
239 upstream to regulate LATS1/2-mediated control over YAP/TAZ, targeting of MARK2/3 would likely
240 select for distinct resistance mechanisms from drugs targeting the TEAD:YAP/TAZ interaction (66).
241 While the liabilities of each targeting strategy await further description in pre-clinical models and
242 ongoing clinical studies, our study justifies consideration of MARK2/3 as an oncoprotein-like cancer
243 target in a diverse collection of human carcinomas and sarcomas harboring hyper-active YAP/TAZ
244 function.

245 Methods

246 Cell culture

247 The HPAF-II, AsPC-1, PANC-1, MIA PaCa-2, NCI-H1299, A549, NCI-H23, RD, MDA-MB231, NCI-
248 H1048, NCI-H211, NCI-H209, NCI-H1836, NCI-H1436, CHL-1, OCI-AML3, THP-1, HEK-293T and
249 K-562 were purchased from American Type Culture Collection (ATCC).

250 The YAPC, PATU8902, PATU8988T, NOMO-1, HEL, SET-2, RH-30, OCI-AML3 and MOLM13 cell
251 lines were purchased from the “Deutsche Sammlung von Mikroorganismen und Zellkulturen” (DSMZ).
252 The KP2, T3M-4, SUIT-2 and KLM-1 cell lines were purchased from the “Japanese Collection of
253 Research Bioresources Cell Bank” (JCRB). The COR-L311 cell line was purchased from the “European
254 Collection of Authenticated Cell Cultures” (ECACC).

255 All human cell lines were grown in Roswell Park Memorial Institute (RPMI) medium supplemented
256 with 10% fetal bovine serum (FBS) and 1% penicillin/streptomycin (Gibco), if not otherwise indicated.
257 HEK 293T and MDA-MB231 cells were grown in Dulbecco's Modified Eagle Medium (DMEM)
258 medium. NCI-H209, NCI-H1836, NCI-H1436, NCI-H1048 were grown in HITES medium (DMEM
259 media supplemented with 5% FBS, 1% penicillin/streptomycin, Insulin-Transferrin-Selenium (Gibco),
260 10 nM Hydrocortisone (Sigma-Aldrich), 10 nM beta-estradiol (Sigma-Aldrich), 10 mM HEPES (Gibco),
261 2mM L-glutamine (Gibco)). All lentiviral packaging with HEK 293T cells and cancer cell line
262 transduction was performed following standard procedures similar to those previously described (27).
263 For organoid culture transduction, single cells were infected using a spin-infection strategy (800g for 2-
264 4h), before virus removal and replating in Matrigel (Corning). All organoids were grown in growth
265 factor reduced Matrigel. Human patient-derived pancreas- and breast cancer organoids were cultured in
266 specific organoid media as described before (67,68).

267

268 Protein lysate preparation for Western blotting and immunoblotting

269 Cells were lysed directly with 2x Laemmli Sample Buffer (BIO-RAD), supplemented with β -
270 mercaptoethanol (Sigma-Aldrich) or in RIPA buffer supplemented with protease inhibitor cocktail
271 (Roche) and Halt Phosphatase inhibitor cocktail (Thermo Fisher). The same total protein amounts or
272 extracts from the same number of cells were loaded into each lane of an SDS-PAGE gel (NuPAGE 4-
273 12% Bis-Tris Protein gels, Thermo Fisher) followed by transfer to a nitrocellulose membrane.
274 Membranes were blocked using 5% non-fat dry milk and washed using TBST following incubation both
275 primary or secondary antibodies. After, membranes were developed with chemiluminescent HRP
276 substrate (Pierce).

277

278 Antibodies used in this study are HRP-conjugated secondary antibodies (rabbit cytochrome c, NA934, 1:5,000
279 – 1:20,000), HRP-conjugated β -actin (Sigma-Aldrich, A3854, 1:5,000), HA (Roche, 3F10, 1:10,000),
280 Flag (Sigma-Aldrich, A8592, 1:5,000), V5 (Invitrogen, R961-25, 1:5,000), myc (Abcam, ab62928,
281 1:3,000), GAPDH (Cell Signaling, D16H11, 1:3,000), H3 (Cell Signaling, D1H2, 1:5,000), GST-tag
282 (Cell Signaling, 5475S, 1:3,000) and primary antibodies MARK2 (Abcam, ab133724, 1:1,000), MARK3
283 (Abcam, ab264285, 1:1,000), YAP (Cell Signaling, D8H1X, 1:1,000), p-YAP/TAZ (S127/S89) (Cell
284 Signaling, D9W2I, 4911, 1:3,000), TAZ (Cell Signaling, E8E9G, D3I6D, 1:1,000), NF2 (Cell Signaling,
285 D1D8, 1:1,000), MST1 (Cell Signaling, 3682T, 1:1,000), MST2 (Cell Signaling, 3952T, 1:1,000),
286 LATS1/2 (GeneTex, GTX87014, 1:1,000), p-LATS1/2 (T1079/T1041) (Cell Signaling, D57D3, Abcam,
287 ab305029, 1:1,000 – 1:3,000), cJUN (Cell Signaling, 60A8, 1:1,000), p-cJUN (S63) (Cell Signaling,
288 E6I7P, 1:1,000), MOB1 (Cell Signaling, E1N9D, 1:1,000), p-MOB1 (T35) (Cell Signaling, 8699T,
289 1:1,000), SAV1 (Cell Signaling, D6M6X, 1:1,000), CDC25C (Cell Signaling, 5H9, 1:1,000), p-CDC25C
290 (S216) (Cell Signaling, 63F9, 1:1,000), Thiophosphate ester (Abcam, ab92570, 1:5,000 – 1:20,000), 14-
291 3-3 (Cell Signaling, 8312S, 1:1,000).

292

293 Apoptosis and cell cycle analysis using flow cytometry

294 For Apoptosis analysis cancer cells transduced with sgRNA constructs were stained using conjugated
295 Annexin-V proteins (Thermo Fisher Scientific) and DAPI according to manufacturer instructions. In
296 brief, 6 days post-infection with lentivirus containing dgRNAs linked to GFP, Cells were detached and
297 resuspended in staining buffer followed by incubation with Annexin-V and DAPI. Stained cells were
298 analyzed by flow cytometry and data analysis was performed with FlowJo software. Early apoptotic-
299 (Annexin-V⁺/DAPI⁻), late apoptotic- (Annexin-V⁺/DAPI⁺), necrotic- (Annexin-V⁻/DAPI⁺) and viable
300 cells (Annexin-V⁻/DAPI⁻) were identified.

301 For cell cycle analysis cancer cells transduced with dgRNA constructs (day 5) were treated with 10 μ M
302 EdU 4h prior to sampling. EdU incorporated into cells was stained according to manufacturer
303 instructions (Thermo Fisher). In brief, Cells were detached and fixed in 4% PFA, permeabilized and
304 EdU conjugated using click chemistry. Stained cells were analyzed by flow cytometry and data analysis
305 was performed with FlowJo software. Cells were identified based on EdU signal and DNA content
306 (DAPI).

307 CRISPR screening and pooled paralog library generation.

308 Library generation

309 The Paralog co-targeting CRISPR library was optimized for the use of SpCas9, a system we recently
310 published(69). Oligonucleotide pools (n=64,697) double guide RNAs targeting 1,719 single gene and
311 2,529 gene combinations were synthesized (Twist Bioscience) with BsmBI cutting sites in between
312 overhang sequences for the dual crRNA fragment. Primers matching the overhang for the lentiviral
313 backbone were used to amplify the oligonucleotide pools. PCR products were purified and cloned using
314 Gibson assembly master mix (New England BioLabs) into LRG3.0, a lentiviral vector with human U6
315 and bovine U6 promoters expressing the two sgRNAs in inverse orientation. To incorporate the dual
316 tracrRNA, the purified tracrRNA fragment was cloned in between the dual crRNAs by a second round
317 of Gibson assembly.

318

319 Paralog library screening

320 To generate stable cell lines, cells were first transduced with a Cas9 vector (Addgene: 108100). Next,
321 cell lines were transduced with the paralog co-targeting CRISPR library virus aiming for a representation
322 of 1,000 cells per sgRNA at a low multiplicity of infection (MOI ~0.3). Briefly, cell lines were
323 transduced by spin infection for 45 min at 600g. On day 3, an initial sample was taken and cells were re-
324 plated maintaining representation. Once 10 cell doublings were reached samples for genomic DNA
325 extraction were again taken.

326

327 Genomic DNA extraction

328 Cells lysed in extraction buffer (10mM Tris, 150mM NaCl, 10mM EDTA, Proteinase K (0.02mg/mL),
329 SDS (0.1%)). Lysates were incubated at 56°C for 48h and genomic DNA was extracted using TRIS-
330 saturated phenol (Thermo Fisher Scientific).

331

332 dgRNA PCR for Illumina sequencing

333 DNA was PCR-amplified and barcoded with P5/P7 primers (Integrated DNA Technologies) using Taq-
334 Gold DNA polymerase (Thermofisher) according to the manufacturer's instructions. Briefly, Taq
335 polymerase, reaction buffer, Magnesium chloride, primers, and 1µg of genomic DNA were mixed and
336 used for each reaction (round 1: PCR for 11 cycles). Amplified DNA was size selected (200-300bp) and
337 barcoded in a second round PCR using stacked P5/P7 primers (round 2: PCR for 9 cycles). The PCR
338 product was sequenced using a paired-end 75 base pair (bp) reads protocol (Illumina).

339

340 Calculation of paralog CRISPR screening \log_2 (fold-change), synergy, P value and FDR

341 Reads were counted by mapping dgRNA sequences to the reference file of the library and a pseudo count
342 of 16 was added. The GEMINI R (v.1.4.0) package was used to calculate \log_2 (fold-changes) (LFC) and
343 synergy scores and statistics with their corresponding P and FDR values (Supplementary Table 2,4-6).

344 In brief, GEMINI calculates the LFC of the dgRNA abundance between initial time point (average
345 abundance of dgRNAs day3 n=10) and the 10-doubling time endpoint. GEMINI has been used to
346 compute the synergy score by comparing the LFCs of each gene pair to the most lethal individual gene
347 of the pair. Non-synergistic pairs were used to calculate FDR and P value. Bayesian analysis and the
348 prior choice were performed as described previously (28).

349 Paralog gene identification and functional domain mapping

350 Paralog pairs were identified by aligning human proteome (>100,000 amino acid sequences) using the
351 Basic Local Alignment Search Tool (BLAST). Matches originating from the same gene were removed.
352 Each top-scored paralog-pair identified (E value < 0.01), that shared the same functional domain of
353 interest was included in the Paralog library. In addition, high-scoring paralogs (E value < 10^{-100}) were
354 included. Functional domains were mapped using Reverse Position-Specific BLAST and the conserved
355 domain database (CDD) (70).

356

357 Selection of sgRNAs and controls

358 Domain annotation and sgRNA positions were compared and sgRNAs cutting in functional domain
359 regions were included in the sgRNA selection pool. sgRNAs with off-targets in paralog genes were
360 removed from the selection pool. Additionally, sgRNAs incompatible with the cloning strategy were
361 removed from the selection pool. sgRNAs were picked based on their off-target score (calculated based
362 on the number of off-target locations in the human genome factored by the fall-off in cutting-efficiency
363 of spCas9 in case of crRNA sequence miss-match). For each gene, 3-4 selective domain-focused sgRNA
364 were picked and combined. A set of sgRNAs targeting known essential genes as positive controls (n=28)
365 and a set of non-targeting (n=97) as well as non-coding region targeting negative controls (n=54) were
366 included in the library. To construct cell line-specific negative controls (non-synergistic pairs), we
367 selected genes that were not expressed in a cell line according to the RNA-seq data
368 ($\log_2(\text{TPM} + 1) < 0.1$).

369

370 Arrayed GFP competition assays

371 For validation, two sgRNAs were synthesized together with bovine U6 promoter as gene blocks
372 (Integrated DNA Technologies) and cloned using Gibson assembly into LRG2.1T (Addgene, 65656).
373 All inserts were verified by Sanger sequencing (Eurofins Genomics). To generate LATS1/2 and MST1/2
374 double knockout pools two sgRNAs co-targeting LATS1/2 or MST1/2 were combined and two sgRNA
375 targeting SAV1, NF2 were combined on one vector. For lentivirus packaging, HEK 293T cells were
376 transfected with sgRNA, pVSVg, psPAX2 plasmids (Addgene, 12260) using PEI reagent (PEI 25000).
377 Percent GFP⁺ populations were followed over time after infection using the Guava EasyCyte flow HT
378 instrument (Millipore). Complete sgRNA sequences are given in Supplementary Table 9.

379

380 Generation of ectopic overexpression vectors

381 All cDNAs were either cloned from Addgene plasmids or synthesized as indicated below. CRISPR-
382 resistant cDNAs were generated either by mutating the PAM sequence or sgRNA binding sites into
383 synonymous codons. All cDNAs were cloned into lentiviral constructs derived from LentiV (Addgene
384 108100), altered to contain internal ribosome entry site (IRES) elements and selection marker resistance
385 genes. For doxycycline induction of cDNA expression, genes were cloned into Doxi-LentiV (derived
386 from Addgene, 80921, 89180 and 71782) vectors and expression was induced using 2 µg/ml
387 doxycycline.

388 MARK2 (Addgene, 23404) and MARK3 (Addgene, 23716) were cloned into the LentiV-IRES vector
389 after the addition of a Flag tag at the N terminus. Hippo pathway genes- LATS1, LATS2, NF2, SAV1,
390 TAZ, MOB1A, MOB1B, MST1, MST2, TEAD1, YAP and GFP, CDC25C, YWHAE (14-3-3ε)
391 encoding V5, HA or myc-tagged cDNAs were from Addgene (66851, 66852, 32834, 32836, 32839) or
392 synthesized (IDT). cDNA encoding for MAP4K1, MAPK4K2, MAPK4K3, MAPK4K4, MAPK4K5,

393 and MAPK4K6, were from Addgene (23484, 23644, 23664, 23486, 23611, 23522) 3xHA tagged and
394 cloned into LentiV. The MAPK4K7 expression vector was built by Vector Builder. All mutations were
395 introduced by geneBlock synthesis or PCR. MKI^{WT} was derived from the coding sequence of CagA
396 (*H.pylori* strain 26695). The sequence containing the EPIYA-repeat regions amino acid position 885-
397 1105 was codon optimized. The cDNA was synthesized and cloned into LentiVi-P2A-GFP or Doxi-
398 LentiV after the addition of a 3xHA or Flag tag at the N terminus. To generate a mutant of MKI with
399 impaired MARK binding capacity (MKI^{MUT}) the leucine 109/143 in the two MARK binding motifs of
400 MKI^{WT} were mutated to glycine.

401

402 Generation of TEAD binding reporter linked to GFP

403 To generate a TEAD-driven GFP reporter, the promoter of the established TEAD binding reporter
404 (8xGTIIC)(18) (Addgene, 34615) was fused into a construct containing destabilized GFP (Addgene,
405 138152).

406 Generation of clonal analog sensitive YAPC cells for growth assays

407 MARK2 analog-sensitive mutants were generated by mutating the gatekeeper amino acid methionine
408 129 to glycine. The functionality of this mutant was confirmed using rescue assays. YAPC cells were
409 infected with cDNA CRISPR resistant to sgMARK2+3 and 3 single cell clones were picked. Mutation
410 of endogenous MARK2 and MARK3 locus for all clones was confirmed using genotyping methods
411 (PCR and nanopore sequencing).

412

413 Cloning, expression, and purification of recombinant proteins

414 ORF encoding human MARK2 (Addgene, 23404) was cloned into pFL system with an N-terminal
415 Strep2SUMO tag. Bacmid was generated using pFL vector using DH10MultiBac cells (Geneva
416 Biotech). Sf9 cells were transfected with purified bacmids. Cells were lysed and rMARK2 was purified
417 using StrepTactin Super flow resin. Protein was aliquoted and snap-frozen at -80°C. Protein

418 concentration was estimated by measuring Abs_{280nm} and samples were assessed by Coomassie staining
419 and MS analysis, confirming the absence of other protein kinases. Recombinant LATS1, LATS2,
420 MARK3 and 14-3-3ε were purchased (Active Motif, 81209, Signalchem, L02-11G, M45-10G, Y75-
421 30H) and purity, correct protein size was confirmed by Coomassie staining.
422 Human ORFs encoding YAP and TAZ were cloned into pGEX4T1 vector with N-terminal GST-tag.
423 BL21-CodonPlus (DE3)-RIPL competent cells (Agilent, 230280) are transformed with sequence-
424 validated vectors. Protein expression was induced with IPTG (GoldBio, I2481C) at 16°C for 18 hours.
425 Bacteria were sedimented, lysed, sonicated and cleared lysates were loaded, washed followed by elution
426 using (50 mM Tris pH 8, 300 mM NaCl, 10% glycerol, 20 mM reduced L-glutathione). Purified proteins
427 were aliquoted and flash-frozen at -80°C. The purity of the proteins was assessed by Coomassie staining.
428 Protein concentration was estimated through Abs_{280nm} measurements.

429

430 In-cell phosphosubstrate identification

431 Gatekeeper mutant MARK2^{M129G} or MARK3^{M132G} cDNA was co-transfected together with cDNAs of
432 individual genes into HEK 293T using polyethyleneimine (PEI). After 24h cells were harvested and
433 incubated for 30 min at 30°C in bulky-ATP-analog (N⁶-Furfuryl-ATP-γ-S) containing Kinase-labeling
434 buffer (Protease inhibitor, 20 mM HEPES, 100 mM potassium acetate, 5mM sodium acetate, 2mM
435 magnesium acetate, 10 mM magnesium chloride, 1mM EGTA, 45 μg/mL Digitonin, 0.5 mM TCEP,
436 5mM GTP, 600 μM ATP, 75 μM N⁶- Furfuryl-ATP-γ-S). Cells were lysed using RIPA buffer (with the
437 addition of 0.1% SDS and 250 U/mL Benzoylase). Thiophosphorylated substrates were alkylated using
438 2.5 mM para-nitrobenzyl mesylate (PNBM) for 10min at RT. Target proteins were affinity purified and
439 analyzed using western blot and anti-thiophosphate ester-specific antibodies.

440

441 Identification of phosphosites using mass spectrometry (MS) and phosphoproteomics.

442 Sample preparation and MS recording

443 Substrate cDNAs were transfected into HEK 293T as described above and sampled 24 h after
444 transfection. Samples were affinity purified using HA-agarose beads (Sigma-Aldrich) and treated with
445 800 U of Lambda Phosphatase (New England Biolabs) for 30 min at 30°C. Beads were washed with RIPA
446 buffer (with Protease inhibitor and Phosphatase inhibitor cocktails). Next, beads bound proteins were
447 incubated for 30min at 30 °C with 3 µg rMARK2 in Kinase-buffer (Tris-HCl pH=7.5, 5 mM MgCl₂, 2
448 mM EGTA, 0.5 mM DTT, 100 µM ATP, Protease- and Phosphatase inhibitor cocktail). Phosphorylated
449 substrates and negative controls were resolved by SDS-PAGE and proteins were stained with Coomassie
450 blue. The bands corresponding to each putative substrate were excised, and gel bands were de-stained.
451 After irreversible alkylation of Cysteine residues, proteins were digested with Trypsin, and peptides were
452 analyzed by LC-MS/MS. Peptides were resolved by nanoscale reversed-phase chromatography and
453 ionized by electrospray (2,200V) into a quadrupole-orbitrap mass spectrometer (Thermo Exploris 480).
454 The MS was set to collect 120,000 resolution precursor scans before data-dependent HCD fragmentation
455 and collection of MS/MS spectra. The area under the curve for chromatographic peaks of precursor
456 peptide ions was used as quantitative metrics for label-free quantification.

457

458 Identification of phosphosites

459 Raw files were analyzed using the Proteome Discoverer environment. For peptide identification, spectra
460 were matched against the UniProt human sequence database, supplemented with common contaminants
461 from the cRAP database and with the sequences of the recombinant proteins expressed as substrates.
462 S/T/Y phosphorylation, N/Q deamidation, and M oxidations were set as variable modifications.
463 Alkylation of C residues with CEMTS was set a static modification. Up to 3 missed trypsin cleavages
464 were allowed. Peptide-spectral matches were filtered using Percolator to maintain 1% FDR using the
465 target-decoy method. The area under the curve defined by peptide ion XIC was integrated and used as a
466 quantitative metric for label-free quantification. To evaluate differential phosphorylation in MARK2-

467 treated samples compared to controls, peptides from each putative substrate were parsed out, and label-
468 free quantification (LFQ) AUC values were used as metrics for relative chemical isoform abundance
469 across conditions. Peptides with no LFQ value in any of the samples were disregarded. For peptides only
470 quantified in one experimental arm, the missing value was imputed using a value smaller than the
471 smallest empirical LFQ in the dataset (value chosen as a proxy for LFQ at detection limit). Relative
472 amounts of phosphorylated peptides in MARK2 treated and control samples were assessed for each
473 chemical isoform independently. Phosphopeptides that were either specifically detected in the MARK2
474 treated samples or showing differential abundance across conditions (>2-fold-change in MARK2 treated
475 vs untreated sample) and whose identity could be confirmed by manual spectral interpretation were
476 prioritized for further validation using in-cell phosphosubstrate identification strategy described above.
477 The fragmentation spectra supporting peptide identity and phosphorylation localization together with the
478 extracted precursor ion chromatogram (XIC) can be found in Supplementary material MS.

479

480 Crystal violet staining

481 Cas9-expressing cancer cells were infected with lentivirus. After 3 days GFP percentage was determined
482 using flow cytometry. GFP⁺ cells were seeded into 24 well plates at a density of 5,000/well. Cells were
483 selected and grown for 10-12 days in the presence of 10µg/mL Blasticidin for controls to reach near
484 confluency. Media was changed every 3 days. Cells were fixed using 4% paraformaldehyde for 15 min
485 followed by staining with Crystal violet (1mg/mL in 90/10% Water/Ethanol) for 5 min. Wells were
486 washed 4 times with water and plates were imaged.

487

488 Subcellular fractionation assay

489 Following perturbation, cancer cells were treated with 500µM cytosolic extraction buffer (10mM
490 HEPES, 10mM KCl, 1mM DTT, 0.1 mM EDTA, 0.1mM EGTA) for 10min on ice. Cells were vortexed
491 for 10sec after the addition of NP40 (final 0.65%) to allow hypotonic cell membrane lysis, followed by

492 5 min 1,500 g centrifugation at 4°C. Cytosolic fraction was removed and pelleted nuclei were lysed in
493 RIPA buffer supplemented with 250 U/mL Benzodase and Protease- and Phosphatase inhibitor cocktail.

494

495 Co-Immunoprecipitation assays

496 HEK 293T cells were transfected with vectors expressing myc-LATS1, myc-LATS2, V5-14-3-3 or V5-
497 NF2 together with Flag-MARK2, Flag-MARK2^{K82H} or Flag-MARK3 and wild-type or mutant HA-
498 tagged substrate cDNAs. For immunoprecipitation, cells were lysed in NP40 buffer (20 mM of Tris-HCl,
499 100 mM of NaCl, 1% NP40, 2 mM of EDTA, Protease- and Phosphatase inhibitor cocktail) or RIPA
500 buffer (Thermo Fisher Scientific) for 10 min at 4 °C. Protein lysates were then centrifuged at 13,000g
501 for 15 min at 4 °C. The supernatant was then transferred to new collection tubes and incubated with to
502 30 µl of prewashed anti-myc or -V5 beads (Chromotek) and equilibrated to a final volume of 1000 µl by
503 adding lysis buffer. Precipitation was performed at 4 °C overnight and washed 4-5 times with lysis
504 buffer. Samples were eluted by boiling for 10 min in 2x Laemmli Sample Buffer supplemented with β-
505 mercaptoethanol.

506 In vitro phosphorylation and interaction assay

507 Bacterial purified recombinant GST-YAP or GST-TAZ were pre-incubated for 30min at 30 °C with
508 recombinant MARK2 or MARK3 in Kinase buffer followed by incubation with either recombinant
509 LATS1 or LATS2 for an additional 30min. Phosphorylated YAP or TAZ were then incubated with
510 6xHis-14-3-3 bound to Ni-NTA affinity resin for 4-16h followed by washing and samples elution.

511

512 RNA-seq, CUT&RUN sample preparation and library construction

513 For RNA-Seq libraries, total RNA was prepared using TRIzol reagent according to the manufacturer's
514 protocol (Thermo Fisher Scientific). Libraries were constructed with the TruSeq Sample Prep Kit v2
515 (Illumina) following the manufacturer's protocol. Briefly, 2 µg of total RNA was used for Poly-A
516 enrichment, fragmentation, cDNA synthesis, end repairing, A tailing, adapter ligation and library

517 amplification. For CUT&RUN, antibody-guided DNA cleavage was performed using the CUTANA
518 CUT&RUN kit (EpiCyper) according to the manufacturer's instructions. Briefly, 500,000 knockout cells
519 were crosslinked for 1 min using 1% paraformaldehyde (PFA) and quenched using Glycine for min. Pre-
520 washing buffer was used with detergents (0.05% SDS and 0.2% Triton X-100). Antibodies used were
521 H3K27ac and IgG (EpiCyper, 13-0045;13-0042). Libraries were constructed with the NEBNext Ultra II
522 DNA Library Prep Kit (New England BioLabs) following the manufacturer's low DNA protocol.
523 Briefly, complete CUT&RUN DNA extracts were spiked-in with E. coli DNA fragments and subjected
524 to end repair, A tailing and adapter ligation (at 1/25 dilution) followed by PCR amplification. Libraries
525 were purified using AMPureXP beads before and after PCR. Barcoded libraries were sequenced using
526 an Illumina Nextseq.

527

528 Bioinformatics- RNA-seq, GSEA, ChIP-seq analysis

529 Basal expression levels, copy number variations and mutations

530 For cell lines basal expression data (TPM) and copy number variations (CNV) absolute values from the
531 cancer cell line encyclopedia (CCLE)(71) were used. RNA-seq data for KLM-1 was obtained from
532 GSE140484. Mutational information from both the CCLE and Cosmic databases was used (72). TNBC
533 and PDAC organoid CNV data were previously published (67)(68).

534 RNA-Seq analysis

535 Raw reads were pseudo-aligned to the transcriptome of the human genome (hg38) using Kallisto (73)
536 with bootstrap 100. For differential gene expression analysis, pseudoalignment counts were read into
537 DESeq2, comparing samples vs control (Ctrl^{KO}) with two replicates for each sample. The differential
538 expression gene analysis was performed using a gene expression cutoff of >0.5 TPM. Results from
539 multiple sequencing runs were batch-corrected using the R package (sva), before count normalization,
540 transformation, and z-score calculation. For heatmap, z-scores of normalized counts from significantly

541 (adjusted P value $< 10^{-4}$) down or up-regulated ($\log_2(\text{fold-change}) < -1$ or > 2) genes in MARK2+3^{dKO}
542 condition were used and plotted using R package (ComplexHeatmap).

543 CUT&RUN and ChIP-seq analysis

544 Raw reads were aligned to the human genome (hg19) and e.coli genome (K12) using Bowtie2 software
545 in sensitive mode(74). Duplicate reads were removed before peak calling. Deeptools was used to
546 normalize samples to e.coli-DNA spike-in controls. Peaks were identified using MACS2 software (75)
547 using 5% FDR cut-off and broad peak option for histone or narrow peak option for transcription factor-
548 ChIP-seq datasets. H3K27ac peaks identified from Ctrl^{KO} and MARK2+3^{dKO}, YAP+TAZ^{dKO} samples
549 were merged and overlapping peaks were combined. Normalized tag counts were calculated using the
550 Bamliquidator package (<https://github.com/BradnerLab/pipeline>) without read extension and $\log_2(\text{fold-}$
551 $\text{change})$ between control and dKO samples was calculated for each peak. YAP/TAZ sensitive enhancers
552 were defined by bound by H3K27ac signal reduction ($-1.5 > \log_2(\text{fold-change})$) and binding of YAP and
553 TEAD4 in ChIP-seq (only enhancers with relative tag count > 3 in Ctrl samples were used; n=7,896;
554 Supplementary Table 11).

555 ChIP-seq datasets of TEAD4 and YAP from MDAMB231 cells were obtained from public GEO data
556 sets TEAD4 and YAP (GSE66081). Sequencing depth normalized ChIP-seq and CUT&RUN pileup
557 tracks were generated using the UCSC genome browser.

558

559 Generation of YAP/TAZ gene signature and gene set enrichment analysis (GSEA)

560 The differential gene expression gene lists of YAP+TAZ^{dKO} compared to Ctrl^{KO} were ranked and the top
561 200 downregulated genes in YAP+TAZ^{dKO} condition were combined. Gene counts were ranked and
562 genes found in at least 1/3 of models were used to generate a general cancer cell line YAP/TAZ target
563 gene set (n=43) (Supplementary Table 7). Differentially expressed gene lists were further analyzed using
564 gene set enrichment analysis with a weighted GSEA Pre-ranked tool. 1,000 gene set permutations were
565 applied(76) and the common cancer YAP/TAZ target gene set was used to analyze the effects of

566 sgMARK2/3 double guide RNAs on gene expression. All fold-changes are provided in Supplementary
567 Table 10.

568

569 *In vivo* tumor growth assay

570 For tumor growth models, cells were injected into the left or right flank. For Dox-inducible MKI cDNA
571 transduced cells mice were. For conditional MARK inhibition experiments *in vivo*, 1×10^5 TRE3G-
572 MKI^{WT/MUT}-PGK-rtTA3 cancer cells in 100 μ L growth factor reduced Matrigel were transplanted
573 subcutaneously into the left or right flank of NOD.Cg-Prkdc^{scid} Il2rg^{tm1Wjl}/SzJ (NSG) mice. Animals
574 were treated with doxycycline in either drinking water (2 mg/ml with 2% sucrose; Sigma-Aldrich) to
575 induce MKI protein expression. For stable knockout experiments *in vivo*, YAPC cells were transduced
576 with (hU6-sgRNA-bU6-sgRNA)-EFS-GFP-2A-BlastR lentivirus, followed by selection with Blasticidin
577 for 3 days. After, 1×10^5 GFP⁺ viable cells were transplanted subcutaneously in 100 μ L growth factor
578 reduced Matrigel into the right flank of NSG mice. For all subcutaneous xenograft experiments tumor
579 growth was monitored using caliper measurements. The humane study end-point was determined as the
580 control group's average tumor size reaching $> 600 \text{ mm}^3$.

581

582 Proliferation, viability assay

583 For the proliferation assays, cells were seeded at a density of 500 cells per well into 96-well plates. Cells
584 were treated 24h after seeding and cell viability was assessed 5 days after treatment using the Cell Titer-
585 Glo luminescent cell viability assay (Promega). Cells treated with vehicle control DMSO (0.1%) or
586 killing control 10 μ M proteasome inhibitor (MG132). Percent viability was calculated by normalizing
587 RLU to DMSO (0.1%) after subtraction of killing control MG132 (10 μ M) signal.

588 For organoids, 5,000 or 10,000 cells were seeded in a 10% Matrigel/90% organoid media mix and grown
589 for 10 days in the presence or absence of 2 μ g/mL doxycycline, before assessment of viability using the
590 Cell Titer-Glo luminescent cell viability assay (Promega).

591 Animal studies

592 All mouse experiments were approved by the Cold Spring Harbor Animal Care and Use Committee.

593 Animals were treated with doxycycline in drinking water (2 mg/ml with 1% sucrose; Sigma-Aldrich) to

594 induce cDNA expression.

595

596

597 **References**

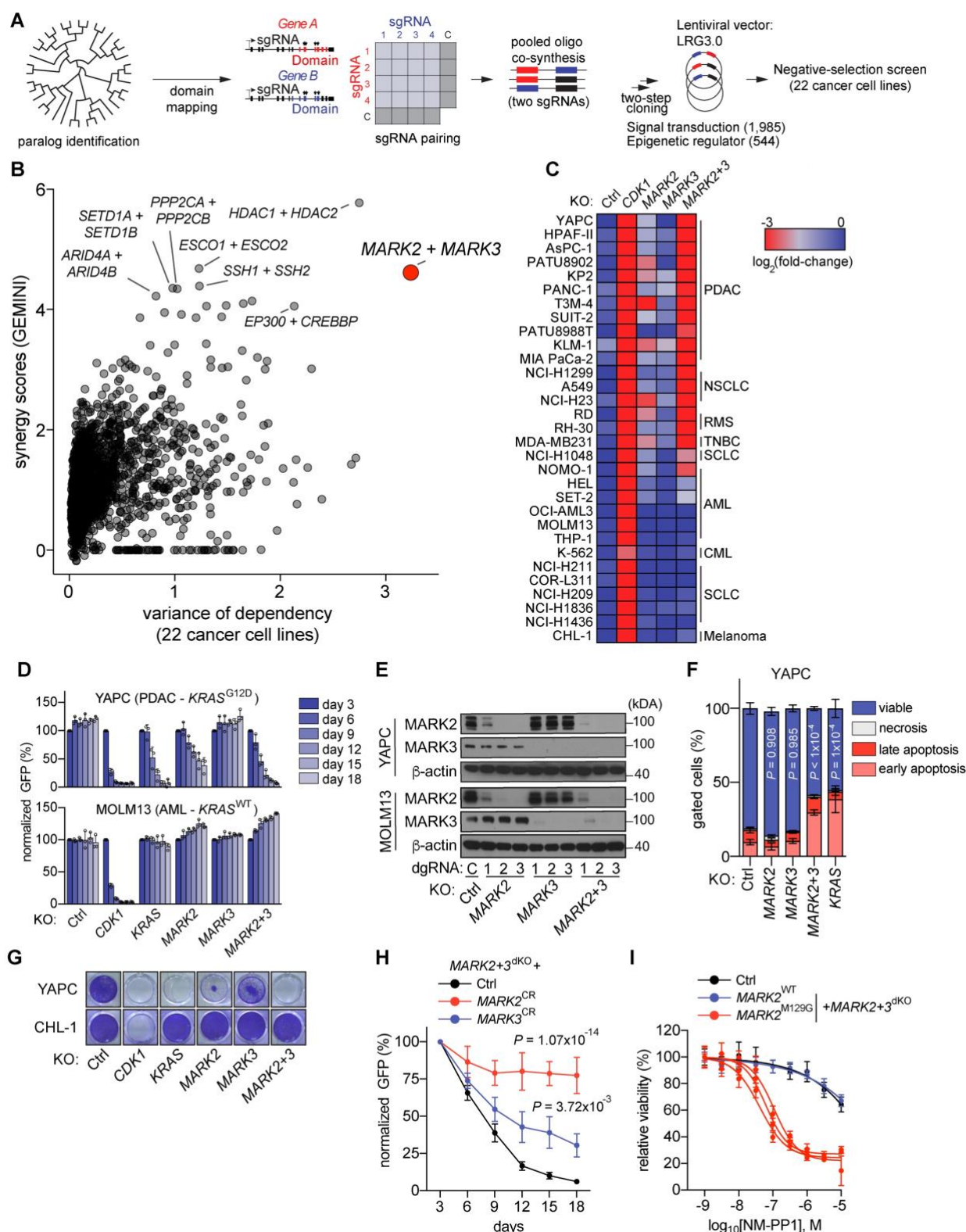
- 598 1. Sanchez-Vega F, Mina M, Armenia J, Chatila WK, Luna A, La KC, *et al.* Oncogenic Signaling
599 Pathways in The Cancer Genome Atlas. *Cell* **2018**;173(2):321-37 e10 doi
600 10.1016/j.cell.2018.03.035.
- 601 2. Zanconato F, Cordenonsi M, Piccolo S. YAP/TAZ at the Roots of Cancer. *Cancer Cell*
602 **2016**;29(6):783-803 doi 10.1016/j.ccell.2016.05.005.
- 603 3. Ma S, Meng Z, Chen R, Guan KL. The Hippo Pathway: Biology and Pathophysiology. *Annu*
604 *Rev Biochem* **2019**;88:577-604 doi 10.1146/annurev-biochem-013118-111829.
- 605 4. Zhao B, Wei X, Li W, Udan RS, Yang Q, Kim J, *et al.* Inactivation of YAP oncoprotein by the
606 Hippo pathway is involved in cell contact inhibition and tissue growth control. *Genes Dev*
607 **2007**;21(21):2747-61 doi 10.1101/gad.1602907.
- 608 5. Huang J, Wu S, Barrera J, Matthews K, Pan D. The Hippo signaling pathway coordinately
609 regulates cell proliferation and apoptosis by inactivating Yorkie, the Drosophila Homolog of
610 YAP. *Cell* **2005**;122(3):421-34 doi 10.1016/j.cell.2005.06.007.
- 611 6. Meng Z, Moroishi T, Mottier-Pavie V, Plouffe SW, Hansen CG, Hong AW, *et al.* MAP4K
612 family kinases act in parallel to MST1/2 to activate LATS1/2 in the Hippo pathway. *Nat*
613 *Commun* **2015**;6:8357 doi 10.1038/ncomms9357.
- 614 7. Zheng Y, Wang W, Liu B, Deng H, Uster E, Pan D. Identification of Happyhour/MAP4K as
615 Alternative Hpo/Mst-like Kinases in the Hippo Kinase Cascade. *Dev Cell* **2015**;34(6):642-55
616 doi 10.1016/j.devcel.2015.08.014.
- 617 8. Li Q, Li S, Mana-Capelli S, Roth Flach RJ, Danai LV, Amcheslavsky A, *et al.* The conserved
618 misshapen-warts-Yorkie pathway acts in enteroblasts to regulate intestinal stem cells in
619 Drosophila. *Dev Cell* **2014**;31(3):291-304 doi 10.1016/j.devcel.2014.09.012.
- 620 9. Li S, Cho YS, Yue T, Ip YT, Jiang J. Overlapping functions of the MAP4K family kinases
621 Hppy and Msn in Hippo signaling. *Cell Discov* **2015**;1:15038 doi 10.1038/celldisc.2015.38.
- 622 10. Zhang N, Bai H, David KK, Dong J, Zheng Y, Cai J, *et al.* The Merlin/NF2 tumor suppressor
623 functions through the YAP oncoprotein to regulate tissue homeostasis in mammals. *Dev Cell*
624 **2010**;19(1):27-38 doi 10.1016/j.devcel.2010.06.015.
- 625 11. Yin F, Yu J, Zheng Y, Chen Q, Zhang N, Pan D. Spatial organization of Hippo signaling at the
626 plasma membrane mediated by the tumor suppressor Merlin/NF2. *Cell* **2013**;154(6):1342-55
627 doi 10.1016/j.cell.2013.08.025.
- 628 12. Zhao B, Ye X, Yu J, Li L, Li W, Li S, *et al.* TEAD mediates YAP-dependent gene induction
629 and growth control. *Genes Dev* **2008**;22(14):1962-71 doi 10.1101/gad.1664408.
- 630 13. Goulev Y, Fauny JD, Gonzalez-Marti B, Flagiello D, Silber J, Zider A. SCALLOPED interacts
631 with YORKIE, the nuclear effector of the hippo tumor-suppressor pathway in Drosophila. *Curr*
632 *Biol* **2008**;18(6):435-41 doi 10.1016/j.cub.2008.02.034.
- 633 14. Zhang H, Liu CY, Zha ZY, Zhao B, Yao J, Zhao S, *et al.* TEAD transcription factors mediate
634 the function of TAZ in cell growth and epithelial-mesenchymal transition. *J Biol Chem*
635 **2009**;284(20):13355-62 doi 10.1074/jbc.M900843200.
- 636 15. Chang L, Azzolin L, Di Biagio D, Zanconato F, Battilana G, Lucon Xiccato R, *et al.* The
637 SWI/SNF complex is a mechanoregulated inhibitor of YAP and TAZ. *Nature*
638 **2018**;563(7730):265-9 doi 10.1038/s41586-018-0658-1.
- 639 16. Mo JS, Meng Z, Kim YC, Park HW, Hansen CG, Kim S, *et al.* Cellular energy stress induces
640 AMPK-mediated regulation of YAP and the Hippo pathway. *Nat Cell Biol* **2015**;17(4):500-10
641 doi 10.1038/ncb3111.
- 642 17. Yang CC, Graves HK, Moya IM, Tao C, Hamaratoglu F, Gladden AB, *et al.* Differential
643 regulation of the Hippo pathway by adherens junctions and apical-basal cell polarity modules.
644 *Proc Natl Acad Sci U S A* **2015**;112(6):1785-90 doi 10.1073/pnas.1420850112.

- 645 18. Dupont S, Morsut L, Aragona M, Enzo E, Giulitti S, Cordenonsi M, *et al.* Role of YAP/TAZ in
646 mechanotransduction. *Nature* **2011**;474(7350):179-83 doi 10.1038/nature10137.
- 647 19. Meng Z, Qiu Y, Lin KC, Kumar A, Placone JK, Fang C, *et al.* RAP2 mediates
648 mechanoresponses of the Hippo pathway. *Nature* **2018**;560(7720):655-60 doi 10.1038/s41586-
649 018-0444-0.
- 650 20. Azzolin L, Panciera T, Soligo S, Enzo E, Bicciato S, Dupont S, *et al.* YAP/TAZ incorporation
651 in the beta-catenin destruction complex orchestrates the Wnt response. *Cell* **2014**;158(1):157-
652 70 doi 10.1016/j.cell.2014.06.013.
- 653 21. Kowalczyk W, Romanelli L, Atkins M, Hillen H, Bravo Gonzalez-Blas C, Jacobs J, *et al.*
654 Hippo signaling instructs ectopic but not normal organ growth. *Science*
655 **2022**;378(6621):eabg3679 doi 10.1126/science.abg3679.
- 656 22. Donato E, Biagioni F, Bisso A, Caganova M, Amati B, Campaner S. YAP and TAZ are
657 dispensable for physiological and malignant haematopoiesis. *Leukemia* **2018**;32(9):2037-40
658 doi 10.1038/s41375-018-0111-3.
- 659 23. Pobbati AV, Han X, Hung AW, Weiguang S, Huda N, Chen GY, *et al.* Targeting the Central
660 Pocket in Human Transcription Factor TEAD as a Potential Cancer Therapeutic Strategy.
661 *Structure* **2015**;23(11):2076-86 doi 10.1016/j.str.2015.09.009.
- 662 24. Bum-Erdene K, Zhou D, Gonzalez-Gutierrez G, Ghozayel MK, Si Y, Xu D, *et al.* Small-
663 Molecule Covalent Modification of Conserved Cysteine Leads to Allosteric Inhibition of the
664 TEAD·Yap Protein-Protein Interaction. *Cell Chem Biol* **2019**;26(3):378-89 e13 doi
665 10.1016/j.chembiol.2018.11.010.
- 666 25. Furet P, Bordas V, Le Douget M, Salem B, Mesrouze Y, Imbach-Weese P, *et al.* The First
667 Class of Small Molecules Potently Disrupting the YAP-TEAD Interaction by Direct
668 Competition. *ChemMedChem* **2022**;17(19):e202200303 doi 10.1002/cmdc.202200303.
- 669 26. Hagenbeek TJ, Zbieg JR, Hafner M, Mroue R, Lacap JA, Sodir NM, *et al.* An allosteric pan-
670 TEAD inhibitor blocks oncogenic YAP/TAZ signaling and overcomes KRAS G12C inhibitor
671 resistance. *Nat Cancer* **2023**;4(6):812-28 doi 10.1038/s43018-023-00577-0.
- 672 27. Shi J, Wang E, Milazzo JP, Wang Z, Kinney JB, Vakoc CR. Discovery of cancer drug targets
673 by CRISPR-Cas9 screening of protein domains. *Nat Biotechnol* **2015**;33(6):661-7 doi
674 10.1038/nbt.3235.
- 675 28. Zamanighomi M, Jain SS, Ito T, Pal D, Daley TP, Sellers WR. GEMINI: a variational Bayesian
676 approach to identify genetic interactions from combinatorial CRISPR screens. *Genome Biol*
677 **2019**;20(1):137 doi 10.1186/s13059-019-1745-9.
- 678 29. Wilting RH, Yanover E, Heideman MR, Jacobs H, Horner J, van der Torre J, *et al.* Overlapping
679 functions of Hdac1 and Hdac2 in cell cycle regulation and haematopoiesis. *EMBO J*
680 **2010**;29(15):2586-97 doi 10.1038/emboj.2010.136.
- 681 30. Welti J, Sharp A, Brooks N, Yuan W, McNair C, Chand SN, *et al.* Targeting the p300/CBP
682 Axis in Lethal Prostate Cancer. *Cancer Discov* **2021**;11(5):1118-37 doi 10.1158/2159-
683 8290.CD-20-0751.
- 684 31. Kawasumi R, Abe T, Arakawa H, Garre M, Hirota K, Branzei D. ESCO1/2's roles in
685 chromosome structure and interphase chromatin organization. *Genes Dev* **2017**;31(21):2136-50
686 doi 10.1101/gad.306084.117.
- 687 32. Zeng Y, Yin L, Zhou J, Zeng R, Xiao Y, Black AR, *et al.* MARK2 regulates chemotherapeutic
688 responses through class IIa HDAC-YAP axis in pancreatic cancer. *Oncogene*
689 **2022**;41(31):3859-75 doi 10.1038/s41388-022-02399-3.
- 690 33. Machino H, Kaneko S, Komatsu M, Ikawa N, Asada K, Nakato R, *et al.* The metabolic stress-
691 activated checkpoint LKB1-MARK3 axis acts as a tumor suppressor in high-grade serous
692 ovarian carcinoma. *Commun Biol* **2022**;5(1):39 doi 10.1038/s42003-021-02992-4.

- 693 34. Ooki T, Murata-Kamiya N, Takahashi-Kanemitsu A, Wu W, Hatakeyama M. High-Molecular-
694 Weight Hyaluronan Is a Hippo Pathway Ligand Directing Cell Density-Dependent Growth
695 Inhibition via PAR1b. *Dev Cell* **2019**;49(4):590-604 e9 doi 10.1016/j.devcel.2019.04.018.
- 696 35. Islam K. The Bump-and-Hole Tactic: Expanding the Scope of Chemical Genetics. *Cell Chem*
697 *Biol* **2018**;25(10):1171-84 doi 10.1016/j.chembiol.2018.07.001.
- 698 36. Wang Y, Xu X, Maglic D, Dill MT, Mojumdar K, Ng PK, *et al.* Comprehensive Molecular
699 Characterization of the Hippo Signaling Pathway in Cancer. *Cell Rep* **2018**;25(5):1304-17 e5
700 doi 10.1016/j.celrep.2018.10.001.
- 701 37. Rausch V, Bostrom JR, Park J, Bravo IR, Feng Y, Hay DC, *et al.* The Hippo Pathway
702 Regulates Caveolae Expression and Mediates Flow Response via Caveolae. *Curr Biol*
703 **2019**;29(2):242-55 e6 doi 10.1016/j.cub.2018.11.066.
- 704 38. Seo E, Basu-Roy U, Gunaratne PH, Coarfa C, Lim DS, Basilico C, *et al.* SOX2 regulates
705 YAP1 to maintain stemness and determine cell fate in the osteo-adipo lineage. *Cell Rep*
706 **2013**;3(6):2075-87 doi 10.1016/j.celrep.2013.05.029.
- 707 39. Huang HL, Wang S, Yin MX, Dong L, Wang C, Wu W, *et al.* Par-1 regulates tissue growth by
708 influencing hippo phosphorylation status and hippo-salvador association. *PLoS Biol*
709 **2013**;11(8):e1001620 doi 10.1371/journal.pbio.1001620.
- 710 40. Heidary Arash E, Shibani A, Song S, Attisano L. MARK4 inhibits Hippo signaling to promote
711 proliferation and migration of breast cancer cells. *EMBO Rep* **2017**;18(3):420-36 doi
712 10.15252/embr.201642455.
- 713 41. Hertz NT, Wang BT, Allen JJ, Zhang C, Dar AC, Burlingame AL, *et al.* Chemical genetic
714 approach for kinase-substrate mapping by covalent capture of thiophosphopeptides and analysis
715 by mass spectrometry. *Curr Protoc Chem Biol* **2010**;2(1):15-36 doi
716 10.1002/9780470559277.ch090201.
- 717 42. Ogg S, Gabrielli B, Piwnicka-Worms H. Purification of a serine kinase that associates with and
718 phosphorylates human Cdc25C on serine 216. *J Biol Chem* **1994**;269(48):30461-9.
- 719 43. Tang X, Jang SW, Wang X, Liu Z, Bahr SM, Sun SY, *et al.* Akt phosphorylation regulates the
720 tumour-suppressor merlin through ubiquitination and degradation. *Nat Cell Biol*
721 **2007**;9(10):1199-207 doi 10.1038/ncb1641.
- 722 44. Yu FX, Zhao B, Panupinthu N, Jewell JL, Lian I, Wang LH, *et al.* Regulation of the Hippo-
723 YAP pathway by G-protein-coupled receptor signaling. *Cell* **2012**;150(4):780-91 doi
724 10.1016/j.cell.2012.06.037.
- 725 45. Larhammar M, Huntwork-Rodriguez S, Rudhard Y, Sengupta-Ghosh A, Lewcock JW. The
726 Ste20 Family Kinases MAP4K4, MINK1, and TNIK Converge to Regulate Stress-Induced
727 JNK Signaling in Neurons. *J Neurosci* **2017**;37(46):11074-84 doi 10.1523/JNEUROSCI.0905-
728 17.2017.
- 729 46. Kanai F, Marignani PA, Sarbassova D, Yagi R, Hall RA, Donowitz M, *et al.* TAZ: a novel
730 transcriptional co-activator regulated by interactions with 14-3-3 and PDZ domain proteins.
731 *EMBO J* **2000**;19(24):6778-91 doi 10.1093/emboj/19.24.6778.
- 732 47. Hong AW, Meng Z, Yuan HX, Plouffe SW, Moon S, Kim W, *et al.* Osmotic stress-induced
733 phosphorylation by NLK at Ser128 activates YAP. *EMBO Rep* **2017**;18(1):72-86 doi
734 10.15252/embr.201642681.
- 735 48. Moon S, Kim W, Kim S, Kim Y, Song Y, Bilousov O, *et al.* Phosphorylation by NLK inhibits
736 YAP-14-3-3-interactions and induces its nuclear localization. *EMBO Rep* **2017**;18(1):61-71 doi
737 10.15252/embr.201642683.
- 738 49. Saadat I, Higashi H, Obuse C, Umeda M, Murata-Kamiya N, Saito Y, *et al.* *Helicobacter pylori*
739 CagA targets PAR1/MARK kinase to disrupt epithelial cell polarity. *Nature*
740 **2007**;447(7142):330-3 doi 10.1038/nature05765.

- 741 50. Nestic D, Miller MC, Quinkert ZT, Stein M, Chait BT, Stebbins CE. Helicobacter pylori CagA
742 inhibits PAR1-MARK family kinases by mimicking host substrates. Nat Struct Mol Biol
743 **2010**;17(1):130-2 doi 10.1038/nsmb.1705.
- 744 51. Pearson JD, Huang K, Pacal M, McCurdy SR, Lu S, Aubry A, *et al.* Binary pan-cancer classes
745 with distinct vulnerabilities defined by pro- or anti-cancer YAP/TEAD activity. Cancer Cell
746 **2021**;39(8):1115-34 e12 doi 10.1016/j.ccell.2021.06.016.
- 747 52. Shue YT, Drainas AP, Li NY, Pearsall SM, Morgan D, Sinnott-Armstrong N, *et al.* A
748 conserved YAP/Notch/REST network controls the neuroendocrine cell fate in the lungs. Nat
749 Commun **2022**;13(1):2690 doi 10.1038/s41467-022-30416-2.
- 750 53. Cottini F, Hideshima T, Xu C, Sattler M, Dori M, Agnelli L, *et al.* Rescue of Hippo coactivator
751 YAP1 triggers DNA damage-induced apoptosis in hematological cancers. Nat Med
752 **2014**;20(6):599-606 doi 10.1038/nm.3562.
- 753 54. Piccolo S, Panciera T, Contessotto P, Cordenonsi M. YAP/TAZ as master regulators in cancer:
754 modulation, function and therapeutic approaches. Nat Cancer **2023**;4(1):9-26 doi
755 10.1038/s43018-022-00473-z.
- 756 55. Battilana G, Zanconato F, Piccolo S. Mechanisms of YAP/TAZ transcriptional control. Cell
757 Stress **2021**;5(11):167-72 doi 10.15698/cst2021.11.258.
- 758 56. Kempthues KJ, Priess JR, Morton DG, Cheng NS. Identification of genes required for
759 cytoplasmic localization in early *C. elegans* embryos. Cell **1988**;52(3):311-20 doi
760 10.1016/s0092-8674(88)80024-2.
- 761 57. Shulman JM, Benton R, St Johnston D. The Drosophila homolog of *C. elegans* PAR-1
762 organizes the oocyte cytoskeleton and directs oskar mRNA localization to the posterior pole.
763 Cell **2000**;101(4):377-88 doi 10.1016/s0092-8674(00)80848-x.
- 764 58. Mohseni M, Sun J, Lau A, Curtis S, Goldsmith J, Fox VL, *et al.* A genetic screen identifies an
765 LKB1-MARK signalling axis controlling the Hippo-YAP pathway. Nat Cell Biol
766 **2014**;16(1):108-17 doi 10.1038/ncb2884.
- 767 59. Kaneda A, Seike T, Danjo T, Nakajima T, Otsubo N, Yamaguchi D, *et al.* The novel potent
768 TEAD inhibitor, K-975, inhibits YAP1/TAZ-TEAD protein-protein interactions and exerts an
769 anti-tumor effect on malignant pleural mesothelioma. Am J Cancer Res **2020**;10(12):4399-415.
- 770 60. Dey A, Varelas X, Guan KL. Targeting the Hippo pathway in cancer, fibrosis, wound healing
771 and regenerative medicine. Nat Rev Drug Discov **2020**;19(7):480-94 doi 10.1038/s41573-020-
772 0070-z.
- 773 61. Vivace Therapeutics I. Study to Evaluate VT3989 in Patients With Metastatic Solid Tumors
774 Enriched for Tumors With NF2 Gene Mutations.
775 <https://classic.clinicaltrials.gov/show/NCT04665206>; 2021.
- 776 62. Oncology I. Oral TEAD Inhibitor Targeting the Hippo Pathway in Subjects With Advanced
777 Solid Tumors. <https://classic.clinicaltrials.gov/show/NCT05228015>; 2022.
- 778 63. Cohen P, Cross D, Janne PA. Kinase drug discovery 20 years after imatinib: progress and
779 future directions. Nat Rev Drug Discov **2021**;20(7):551-69 doi 10.1038/s41573-021-00195-4.
- 780 64. Lu H, Zhou Q, He J, Jiang Z, Peng C, Tong R, *et al.* Recent advances in the development of
781 protein-protein interactions modulators: mechanisms and clinical trials. Signal Transduct
782 Target Ther **2020**;5(1):213 doi 10.1038/s41392-020-00315-3.
- 783 65. Olah J, Szenasi T, Lehotzky A, Norris V, Ovadi J. Challenges in Discovering Drugs That
784 Target the Protein-Protein Interactions of Disordered Proteins. Int J Mol Sci **2022**;23(3) doi
785 10.3390/ijms23031550.
- 786 66. Sun Y, Hu L, Tao Z, Jarugumilli GK, Erb H, Singh A, *et al.* Pharmacological blockade of
787 TEAD-YAP reveals its therapeutic limitation in cancer cells. Nat Commun **2022**;13(1):6744
788 doi 10.1038/s41467-022-34559-0.

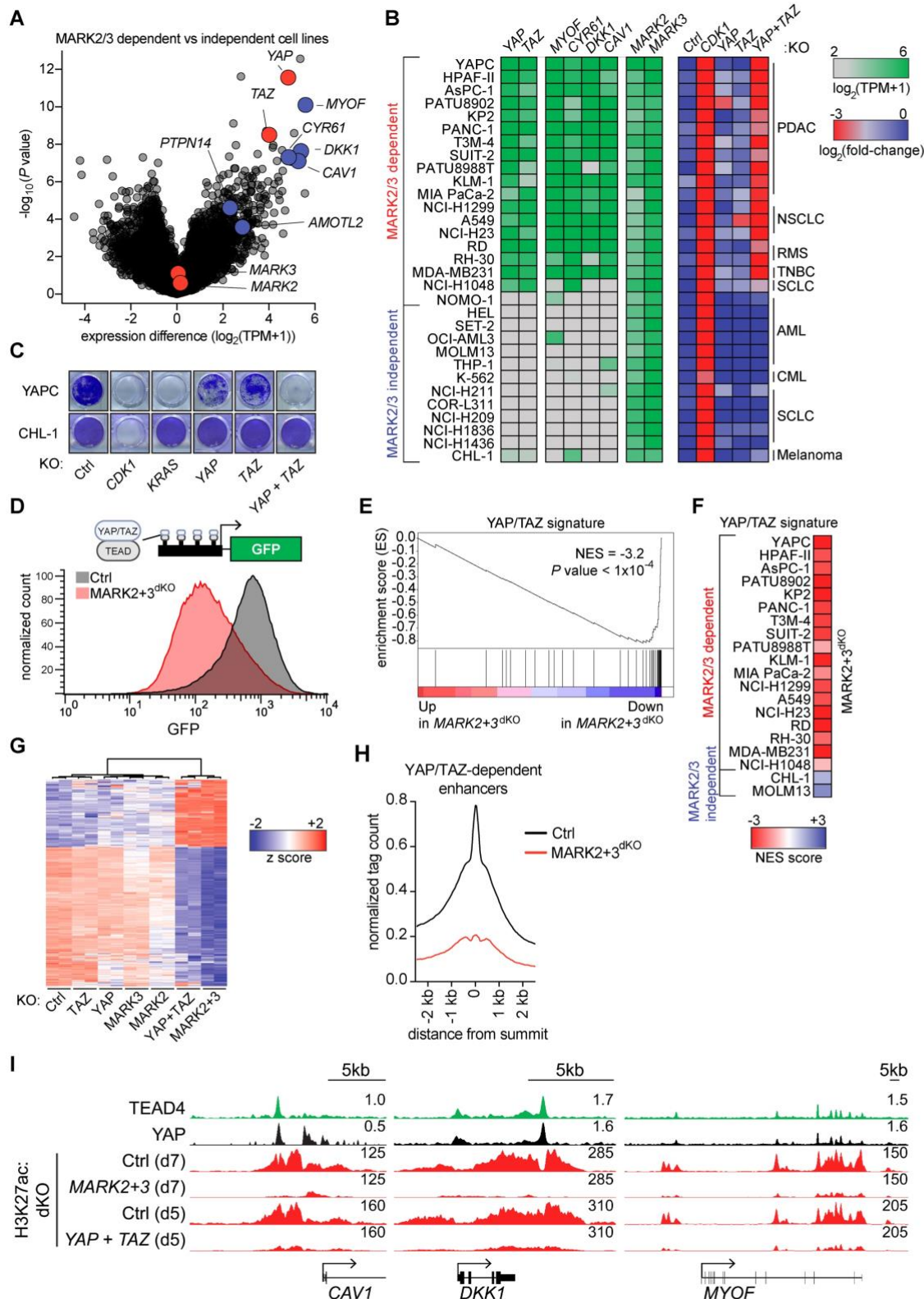
- 789 67. Tiriac H, Belleau P, Engle DD, Plenker D, Deschenes A, Somerville TDD, *et al.* Organoid
790 Profiling Identifies Common Responders to Chemotherapy in Pancreatic Cancer. *Cancer*
791 *Discov* **2018**;8(9):1112-29 doi 10.1158/2159-8290.CD-18-0349.
- 792 68. Bhatia S, Kramer M, Russo S, Naik P, Arun G, Brophy K, *et al.* Patient-Derived Triple-
793 Negative Breast Cancer Organoids Provide Robust Model Systems That Recapitulate Tumor
794 Intrinsic Characteristics. *Cancer Res* **2022**;82(7):1174-92 doi 10.1158/0008-5472.CAN-21-
795 2807.
- 796 69. Li R, Klingbeil O, Monducci D, Young MJ, Rodriguez DJ, Bayyat Z, *et al.* Comparative
797 optimization of combinatorial CRISPR screens. *Nat Commun* **2022**;13(1):2469 doi
798 10.1038/s41467-022-30196-9.
- 799 70. Marchler-Bauer A, Derbyshire MK, Gonzales NR, Lu S, Chitsaz F, Geer LY, *et al.* CDD:
800 NCBI's conserved domain database. *Nucleic Acids Res* **2015**;43(Database issue):D222-6 doi
801 10.1093/nar/gku1221.
- 802 71. Barretina J, Caponigro G, Stransky N, Venkatesan K, Margolin AA, Kim S, *et al.* The Cancer
803 Cell Line Encyclopedia enables predictive modelling of anticancer drug sensitivity. *Nature*
804 **2012**;483(7391):603-7 doi 10.1038/nature11003.
- 805 72. Tate JG, Bamford S, Jubb HC, Sondka Z, Beare DM, Bindal N, *et al.* COSMIC: the Catalogue
806 Of Somatic Mutations In Cancer. *Nucleic Acids Res* **2019**;47(D1):D941-D7 doi
807 10.1093/nar/gky1015.
- 808 73. Bray NL, Pimentel H, Melsted P, Pachter L. Near-optimal probabilistic RNA-seq
809 quantification. *Nat Biotechnol* **2016**;34(5):525-7 doi 10.1038/nbt.3519.
- 810 74. Langmead B, Salzberg SL. Fast gapped-read alignment with Bowtie 2. *Nat Methods*
811 **2012**;9(4):357-9 doi 10.1038/nmeth.1923.
- 812 75. Feng J, Liu T, Qin B, Zhang Y, Liu XS. Identifying ChIP-seq enrichment using MACS. *Nat*
813 *Protoc* **2012**;7(9):1728-40 doi 10.1038/nprot.2012.101.
- 814 76. Subramanian A, Tamayo P, Mootha VK, Mukherjee S, Ebert BL, Gillette MA, *et al.* Gene set
815 enrichment analysis: a knowledge-based approach for interpreting genome-wide expression
816 profiles. *Proc Natl Acad Sci U S A* **2005**;102(43):15545-50 doi 10.1073/pnas.0506580102.



817

818 **Fig. 1. Paralog co-targeting CRISPR screens identify MARK2/3 as context-specific cancer**
 819 **dependencies.** A,B, Workflow of paralog double knockout CRISPR screens including paralog
 820 identification, domain mapping, sgRNA design, oligo synthesis, cloning, and negative selection
 821 screening. Numbers of paralog combinations are indicated. B, CRISPR screening results

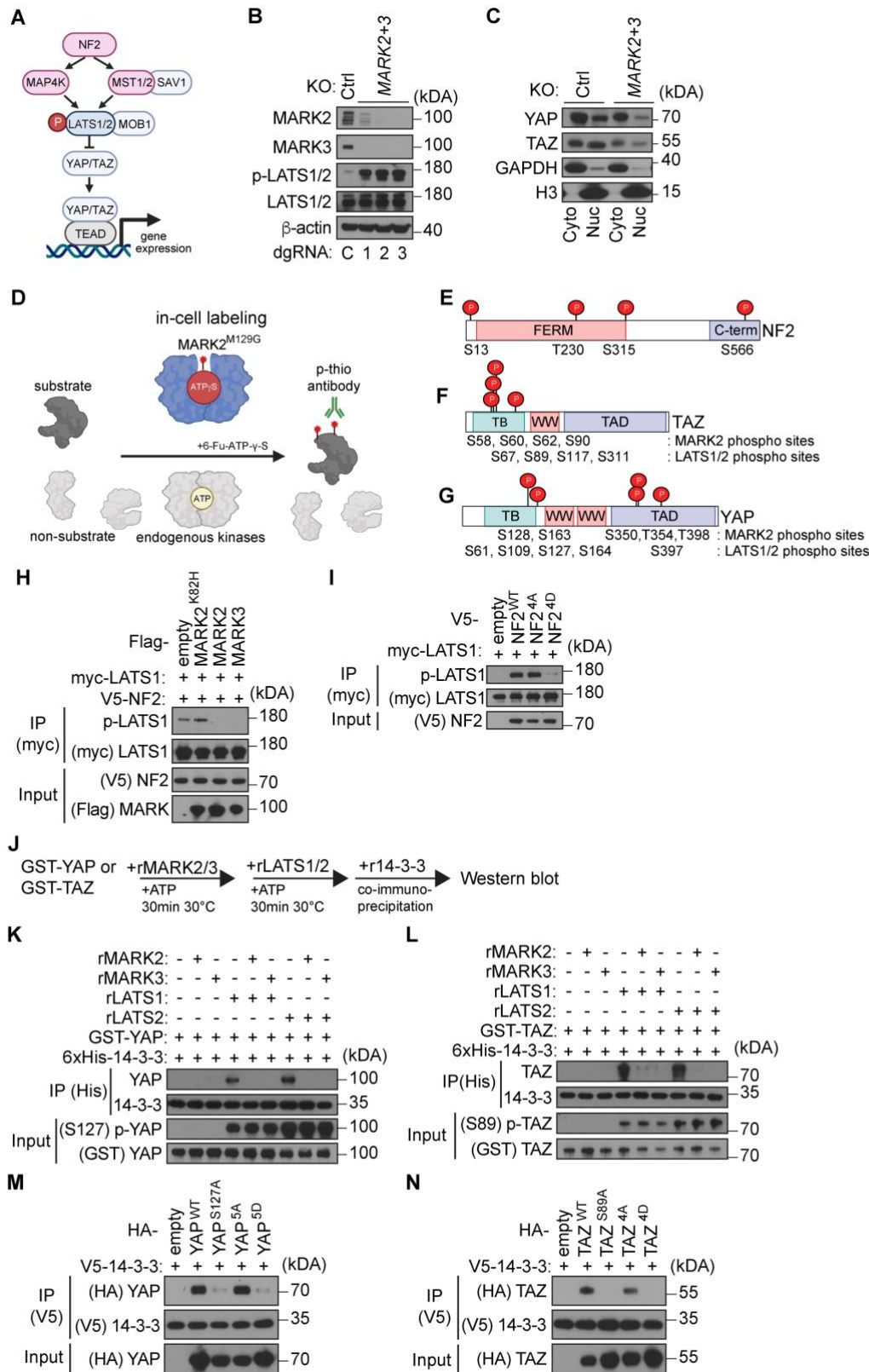
822 summary, analysis of synergy between paralog gene pairs (GEMINI score) (**Supplementary Table**
823 1,2,4-6) maximum scores are shown together with variance of dependency (variance of average
824 \log_2 (fold-change) of double guide RNA abundance) across 22 cell lines screened. Each dot represents a
825 double knockout paralog-pair (n=2,726) among signaling- and epigenetic regulators. **C,D**, Competition-
826 based fitness assays in Cas9-expressing cancer cells after lentiviral knockout of indicated genes
827 (expression of double guide RNAs (dgRNA) was linked to GFP). **c**, Heatmap color indicates the
828 \log_2 (fold-change) of normalized GFP (%GFP⁺ normalized to day 3 or 6 after infection). n=3. **d**,
829 Competition-based fitness assays in the indicated cell lines. Data are shown as mean \pm SD of normalized
830 %GFP⁺ (to day 3 after infection). n=3. **E**, Western blot analysis of the indicated cell lines. **F**, Apoptosis
831 measurements using Annexin-V and DAPI in Cas9-expressing YAPC cells. Indicated genes were
832 knocked out using lentiviral dgRNAs linked to GFP. Data are shown as mean \pm SD. n=3-6. *P* value was
833 calculated on change in viability compared to control with one-way ANOVA and Dunnett's correction.
834 **G**, Crystal violet stain of indicated cells following lentiviral knockout of indicated genes. Data shown
835 are representative of three independent biological replicates. **H**, Rescue experiment in YAPC cells using
836 lentiviral expression of CRISPR resistant (CR) cDNAs or empty vector control (Ctrl). Data shown are
837 the mean \pm SD of %GFP⁺ (normalized to day 3 after infection). n=3. *P* values are calculated using a
838 mixed effects model (considering the interaction of experimental groups over time) compared to Ctrl
839 group and corrected with Bonferroni-Holm (BH). **I**, Normalized relative luminescence units (RLU) from
840 CellTiter-Glo viability measurements of the indicated YAPC cell lines following 5 days of 1NM-PP1
841 treatment. Data are shown as mean \pm SD. n=9 measurements from three biological replicates performed
842 in triplicate. Four-parameter dose-response curves were plotted.
843



844

845 **Fig. 2. MARK2/3 dependency in cancer is linked to the maintenance of YAP/TAZ function.** A,
 846 mRNA expression differences comparing 19 MARK2/3-dependent cell lines to 12 MARK2/3-
 847 independent human cancer cell lines. Transcriptome data were obtained from the CCLE database, KLM-

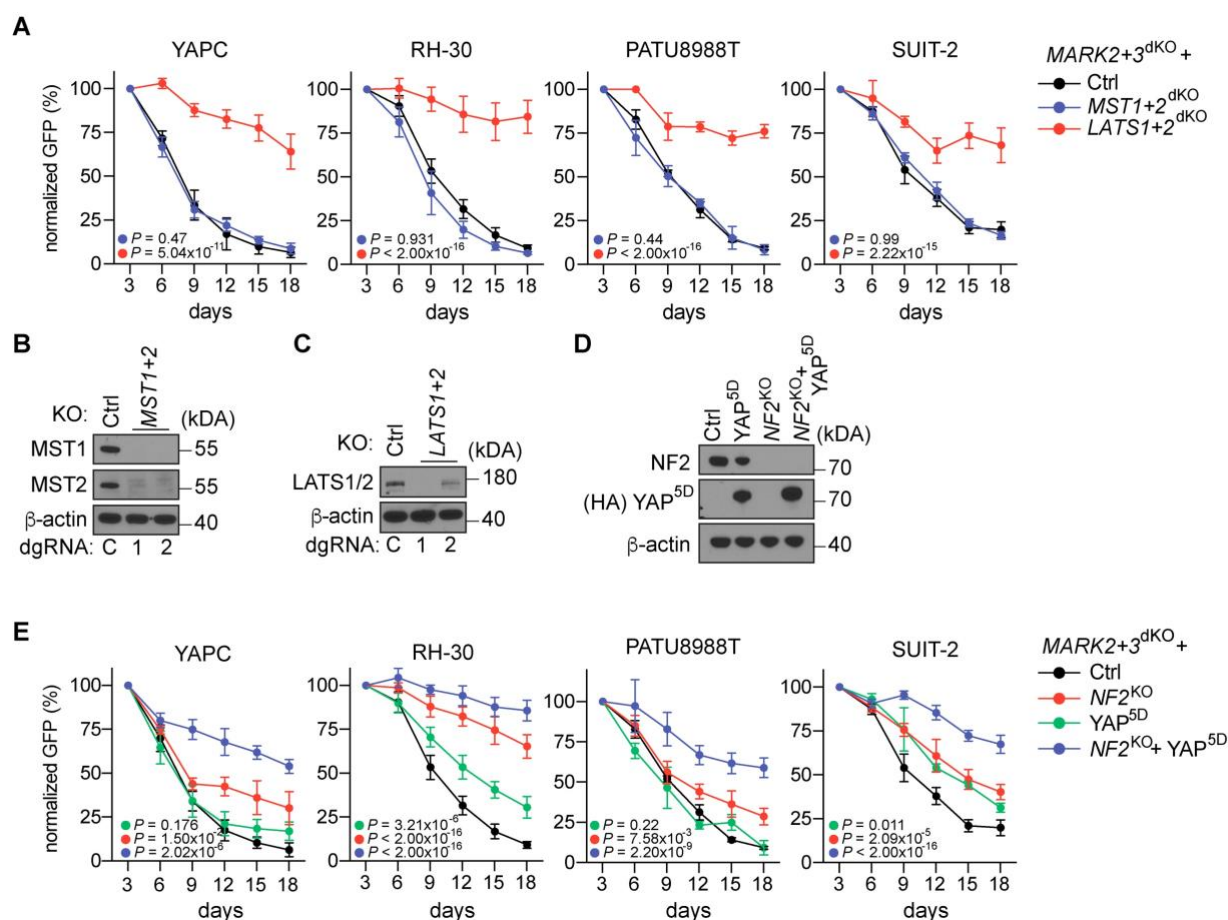
848 1 (GSE140484) and CHL-1 (this paper). TPM, transcripts per million were calculated and the difference
849 in $\log_2(\text{TPM}+1)$ was plotted. *P* values were calculated using Empirical Bayes Statistics (eBayes) for
850 differential expression with BH correction. **B**, Heatmap of MARK2/3 dependent and independent cancer
851 cell lines showing dependence on YAP/TAZ and expression of target genes. Competition-based fitness
852 assays in Cas9-expressing cancer cells after lentiviral knockout of indicated genes (expression of
853 dgRNAs was linked with GFP). Heatmap color indicates the $\log_2(\text{fold-change})$ of %GFP⁺ (normalized
854 to day 3 or 6 after infection). *n*=3. **C**, Crystal violet stain of indicated cells following lentiviral knockout
855 of indicated genes. Data shown are representative of three independent biological replicates. **D**, Flow
856 cytometry histogram of YAP/TAZ:TEAD reporter assay(18) in MDA-MB231 cells, on day 9 post-
857 infection. Data are representative of three independent experiments. **E**, Gene set enrichment analysis
858 (GSEA) of Cas9⁺ MDA-MB231 cancer cells following MARK2+3^{dKO}, including normalized enrichment
859 score (NES) and *P* value. **F**, Heatmap showing the GSEA NES for the YAP/TAZ gene signature
860 following MARK2+3^{dKO} in dependent and independent cell lines. **G**, Heatmap of mRNA expression
861 ($\log_2(\text{normalized count})$) z-scores in Cas9⁺ MDA-MB231 cells of genes significantly down- or up
862 regulated upon MARK2+3^{dKO}. Expression values of down genes (*n*=188) and up genes (*n*=91) of two
863 replicate samples following gene knockout were grouped based on unsupervised clustering. Significant
864 differentially expressed genes were defined as adjusted *P* value $<10^{-4}$ and $\log_2(\text{fold-change}) >2$ or <-1 .
865 *P* values from Wald test (DEseq2) adjusted using BH. **H**, CUT&RUN density profile of YAP:TEAD4
866 bound, YAP/TAZ^{dKO} sensitive H3K27ac marked enhancer loci (*n*=7,896) following MARK2+3^{dKO}.
867 Profiles shown are an average of 50bp bins around the summit of the enhancers. **i**, Occupancy profiles
868 of public Chromatin immunoprecipitation sequencing (ChIP-seq) (TEAD4, YAP) (GSE66083) and
869 CUT&RUN (H3K27ac) upon indicated gene knockout at YAP/TAZ target gene loci.



870

871 **Fig. 3. MARK2/3 catalyze inhibitory phosphorylation of NF2 and activating phosphorylation of**
 872 **YAP/TAZ. A, Illustration of the Hippo pathway. B,C Western blot analysis of Cas9⁺ YAPC cells b,**

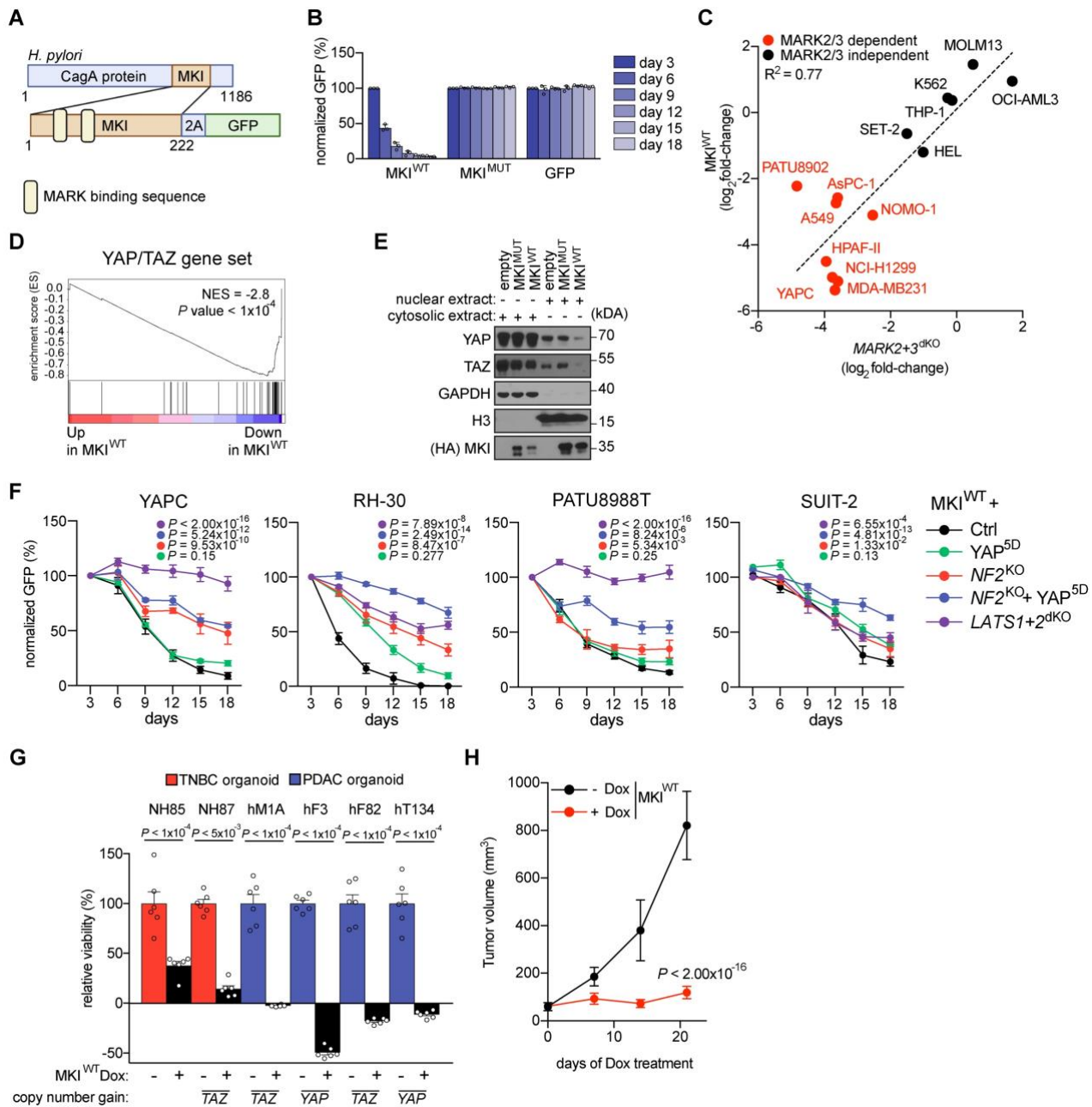
873 whole cell lysate or c, following fractionation into nuclear (Nuc) and cytosolic (Cyto) fraction, following
874 control^{dKO} (Ctrl) or MARK2+3^{dKO}. Independent double guide RNAs (dgRNA) are indicated. **D**,
875 Illustration of in-cell phosphorylation assay. Epitope-tagged cDNA coding for putative MARK2-
876 substrates are transfected into HEK-293T cells together with cDNA coding for analog-sensitive mutant
877 MARK2^{M129G}. Kinase assay is performed using ATP analog (6-Fu-ATP- γ -S) selective for MARK2^{M129G}.
878 Labeled substrates are alkylated using p-nitrobenzyl mesylate (PNBM) and identified following
879 purification by western blot analysis. **E-G**, Lolli-pop illustration of MARK2-dependent phosphorylation
880 sites on NF2, YAP and TAZ identified using mass spectrometry-based phosphoproteomics. C-
881 term=carboxy-terminal domain, TB=TEAD binding domain, TAD=transactivation domain. **H**, IP-
882 western blot analysis evaluating the phosphorylation p-LATS1 (T1079) in presence or absence of
883 MARK2 or MARK3 following NF2 overexpression in HEK-293T cells. Data are representative of two
884 independent experiments. **I**, IP-western blot analysis evaluating the phosphorylation p-LATS1 (T1079)
885 after NF2 mutant overexpression in HEK-293T cells. Data are representative of two independent
886 experiments. **J-L**, *In vitro* phosphorylation assay and IP-western blot analysis, evaluating the interaction
887 of 14-3-3 ϵ and recombinant LATS1 (rLATS1) or LATS2 (rLATS2) phosphorylated GST-YAP or GST-
888 TAZ, following phosphorylation with recombinant MARK2 (rMARK2) or MARK3 (rMARK3). Data
889 are representative of two independent experiments. **M**, IP-western blot analysis evaluating the
890 interaction between 14-3-3 ϵ and YAP^{5D} (phosphomimetic mutant), YAP^{5A} (phospho-null mutant) and
891 controls YAP^{WT} (wild type) and YAP^{S127A} (LATS1/2 phosphosite/ 14-3-3 interaction mutant) in HEK-
892 293T cells. Data are representative of two independent experiments. **N**, IP-western blot analysis
893 evaluating the interaction between 14-3-3 ϵ and TAZ^{4D} (phosphomimetic mutant), TAZ^{4A} (phospho-null
894 mutant) and controls TAZ^{WT} (wild type) and TAZ^{S89A} (LATS1/2 phosphosite/ 14-3-3 interaction mutant)
895 in HEK-293T cells. Data are representative of two independent experiments.
896
897



898

899 **Fig. 4. Regulation of NF2 and YAP accounts for the essential functions of MARK2/3 in human**
 900 **cancer. A,** Rescue experiment of MARK2+3^{dKO} following double knockout of *LATS1/2* or *MST1/2* and
 901 control double knockout Ctrl (dgRNA targeting hROSA26 locus) in indicated Cas9⁺ cell lines. Data
 902 shown are the mean ± SD of %GFP⁺ (normalized to day 3 after infection). n=3-6. *P* values are calculated
 903 using a mixed effects model (considering the interaction of experimental groups over time) compared to
 904 Ctrl group and corrected with Bonferroni-Holm (BH). **B,C** Western blot analysis in YAPC cells and
 905 independent dgRNAs are indicated. **D,** Western blot analysis in Cas9⁺ YAPC cells. **E,** Rescue
 906 experiment of MARK2+3^{dKO} following knockout of *NF2* or Ctrl and lentiviral HA-YAP^{5D}
 907 overexpression. Data shown are the mean ± SD of %GFP⁺ (normalized to day 3 after infection). n=3. *P*
 908 values are calculated using a mixed effects model (considering the interaction of experimental groups
 909 over time) compared to Ctrl group and corrected with Bonferroni-Holm (BH).

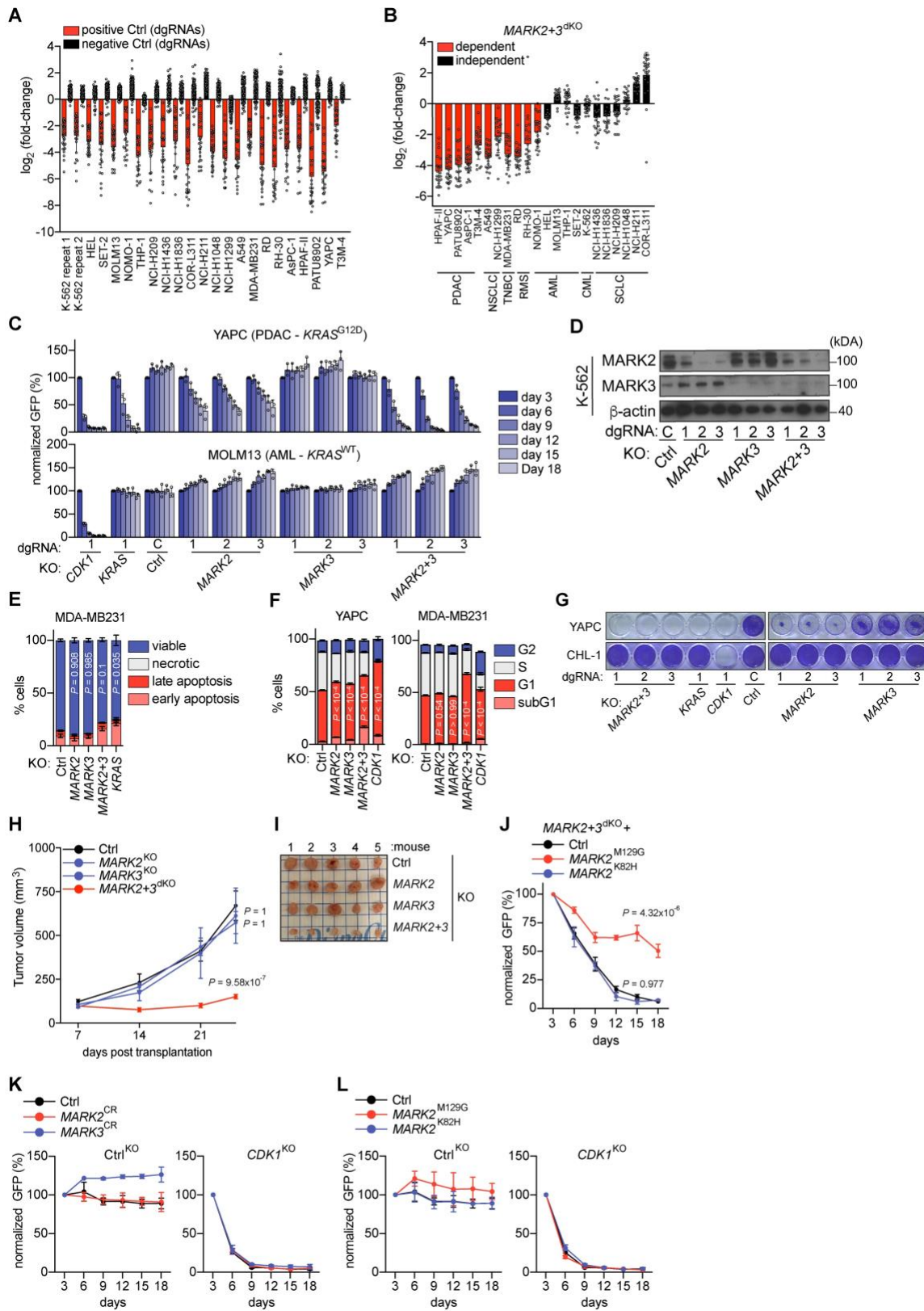
910



911

912 **Fig. 5. Inducible expression of a protein-based MARK2/3 inhibitor re-instates Hippo-mediated**
 913 **tumor suppression in organoid and xenograft tumor models.** **A**, Illustration of MKI protein derived
 914 from *Helicobacter pylori* (*H.pylori*). Positioning of self-cleaving peptides (2A), GFP reporter, and
 915 number of amino acids are indicated. **B**, Competition-based fitness assays in YAPC cells after lentiviral
 916 expression of MKI^{WT} or MKI^{MUT}. **C**, Comparison of log₂(fold-change) of MKI and MARK2+3^{dKO}
 917 double knockout competition data in Cas9⁺ cancer cell lines. Pearson correlation coefficient was
 918 calculated. Data shown are the mean of %GFP⁺ (normalized to day 3 after infection). n=3. **D**, Gene set
 919 enrichment analysis (GSEA) of RNA-seq data from MKI^{WT} compared to MKI^{MUT} expressing MDA-
 920 MB231 cells. Normalized enrichment score (NES) and P value are shown. **E**, Western blot analysis in
 921 YAPC cells 24h following doxycycline induced expression of indicated proteins. **F**, Rescue experiment
 922 of MKI^{WT} expression following knockout of *LATS1/2*, *NF2* or Ctrl (dgRNA targeting hROSA26 locus)
 923 and lentiviral HA-YAP^{5D} overexpression. Data shown are the mean ± SD of %GFP⁺ (normalized to day

924 3 after infection). $n=3$. P values are calculated using a mixed effects model (considering the interaction
925 of experimental groups over time) compared to Ctrl group and corrected with Bonferroni-Holm (BH).
926 **G**, Normalized relative luminescence units (RLU) from CellTiter-Glo viability measurements of the
927 indicated human patient-derived triple-negative breast cancer (TNBC) or pancreatic ductal
928 adenocarcinoma (PDAC) organoids following doxycycline (Dox) induced expression of MKI^{WT} for 10
929 days. Data shown are mean \pm SD. $n=6$ measurements from two biological replicates performed in
930 triplicate. P value was calculated using a two-tailed parametric t-test with Welch's correction. **H**, Growth
931 kinetics of subcutaneous YAPC xenografts implanted in immunodeficient mice. Expression of MKI^{WT}
932 from a doxycycline (Dox)-inducible lentiviral construct was induced on day 10 post-injection of the
933 cells. Data are shown as mean \pm SD. $n=5$ per group. P values are calculated using a mixed effects model
934 (considering the interaction of experimental groups over time) compared to Ctrl group (-Dox) and
935 corrected with Bonferroni-Holm (BH).

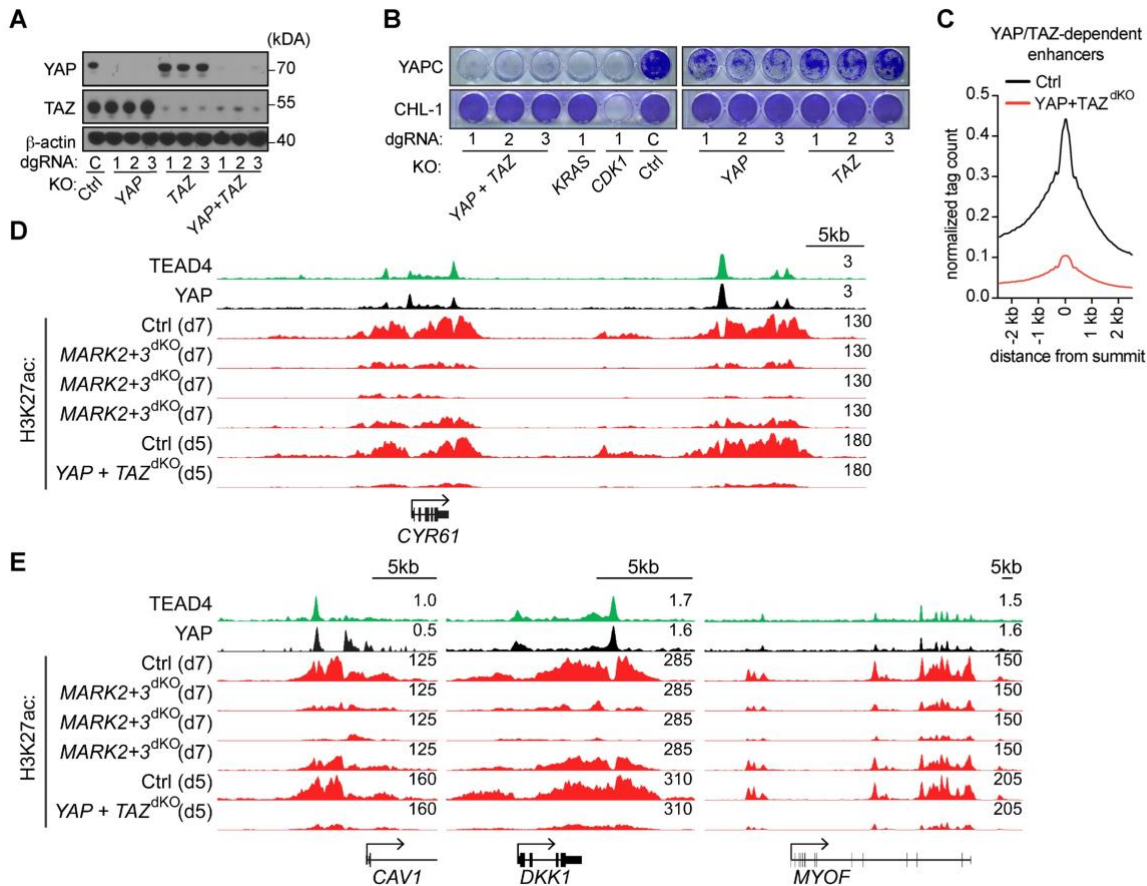


936

937 **Supplementary Fig. S1.**

938 **A,B** CRISPR screening results from 22 cancer cell lines. **A**, Abundance fold-change of positive controls
 939 (dgRNAs targeting essential genes n=28 paired with control) and negative controls (dgRNAs targeting

940 non-coding regions n=54 and nontargeting dgRNAs n=97). Data are shown as mean \pm SD **B**, Abundance
941 fold-change of dgRNAs targeting MARK2+3. Each dot represents a single dgRNA. Data are shown as
942 mean \pm SD n=24 dgRNAs. **C**, Competition-based fitness assays in Cas9-expressing cancer cells after
943 lentiviral knockout of indicated genes with independent dgRNAs (expression of dgRNAs was linked
944 with GFP) (Data shown are an extension of **Fig. 1D**). Data shown are the mean \pm SD of %GFP⁺
945 (normalized to day 3 after infection). n=3. **D**, Western blot analysis of Cas9⁺ K-562 cells. **E**, Analysis of
946 apoptosis assay using Annexin-V and DAPI in Cas9⁺ MDA-MB231 cells. Indicated genes were knocked
947 out using lentiviral dgRNAs linked to GFP. Data are shown as mean \pm SD. n=3-6. *P* value was calculated
948 on change in viability compared to control with one-way ANOVA and Dunnett's correction. **F**, EdU
949 incorporation assays following indicated gene knock out using lentiviral dgRNAs linked to GFP in Cas9⁺
950 indicated cells. Data are shown as mean \pm SD. n=3. *P* value was calculated on change in S-phase
951 population to control with one-way ANOVA and Dunnett's correction. **G**, Crystal violet stain of
952 indicated cells following lentiviral knockout of indicated genes. Data shown are representative of three
953 independent experiments and an extension of **Fig. 1G**. **H**, Growth kinetics of subcutaneous YAPC
954 xenografts implanted in immunodeficient mice. Indicated genes were knocked out just before injection.
955 Data are shown as mean \pm s.e.m. n=5 per group. *P* values are calculated using a mixed effects model
956 (considering the interaction of experimental groups over time) compared to Ctrl group and corrected
957 with Bonferroni-Holm (BH). **I**, Tumor imaging at the end-point of the xenograft experiments shown in
958 **H**. **J**, Rescue experiment in Cas9⁺ YAPC cells using lentiviral overexpression cDNA of CRISPR
959 resistant (CR) analog sensitive mutant *MARK2*^{M129G}, kinase-dead mutant *MARK2*^{K82H} or empty vector
960 control (Ctrl). Data shown are the mean \pm SD of %GFP⁺ (normalized to day 3 after infection). n=3. *P*
961 values are calculated using a mixed effects model (considering the interaction of experimental groups
962 over time) compared to Ctrl group and corrected with Bonferroni-Holm (BH). **K,L** Competition-based
963 fitness assays for Ctrl (dgRNA targeting hROSA26 locus) and knockout of essential gene *CDK1*
964 corresponding to experiments shown in **Fig. 1H** and **J**. Data shown are the mean \pm SD of %GFP⁺
965 (normalized to day 3 after infection). n=3.



966

967

Supplementary Fig. S2.

968

969

970

971

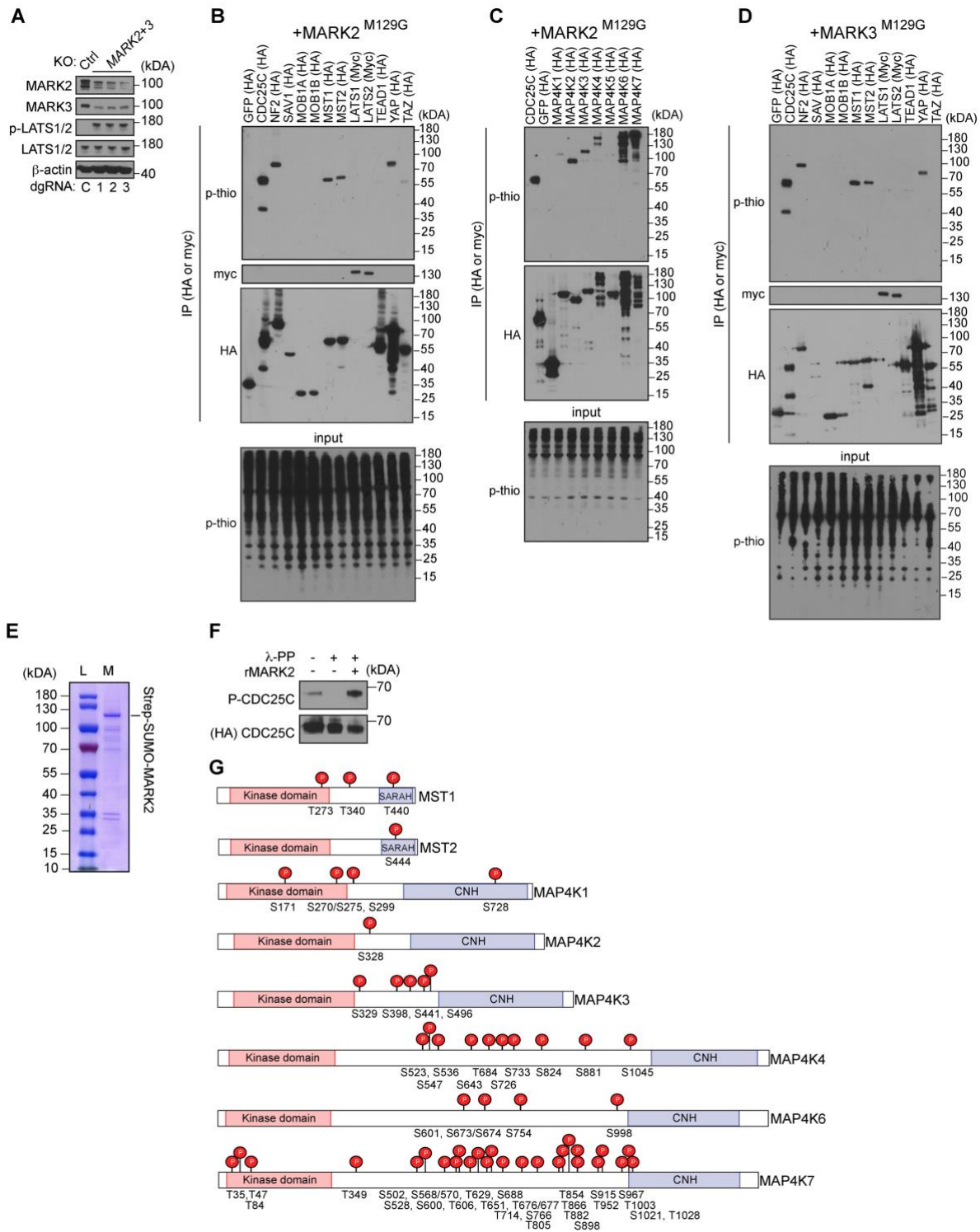
972

973

974

975

A, Western blot analysis in Cas9⁺ YAPC cells. **B**, Crystal violet stain of YAPC and CHL-1 (MARK2/3 independent) cells following dgRNA assisted lentiviral knockout of indicated genes. Data are representative of three independent experiments. **c**, CUT&RUN density profile of YAP/TAZ sensitive H3K27ac marked enhancer loci (n=7,896) following YAP+TAZ^{dKO}. Profiles shown are an average of 50bp bins around the summit of the enhancers. **D,E** Occupancy profiles of public Chromatin immunoprecipitation sequencing (ChIP-seq) (TEAD4, YAP) (GSE66083) and CUT & RUN (H3K27ac) upon indicated gene knockout at YAP/TAZ target gene loci. (Three different dgRNAs for each *MARK2* and *MARK3*) (Data shown are an extension of **Fig. 2I**).

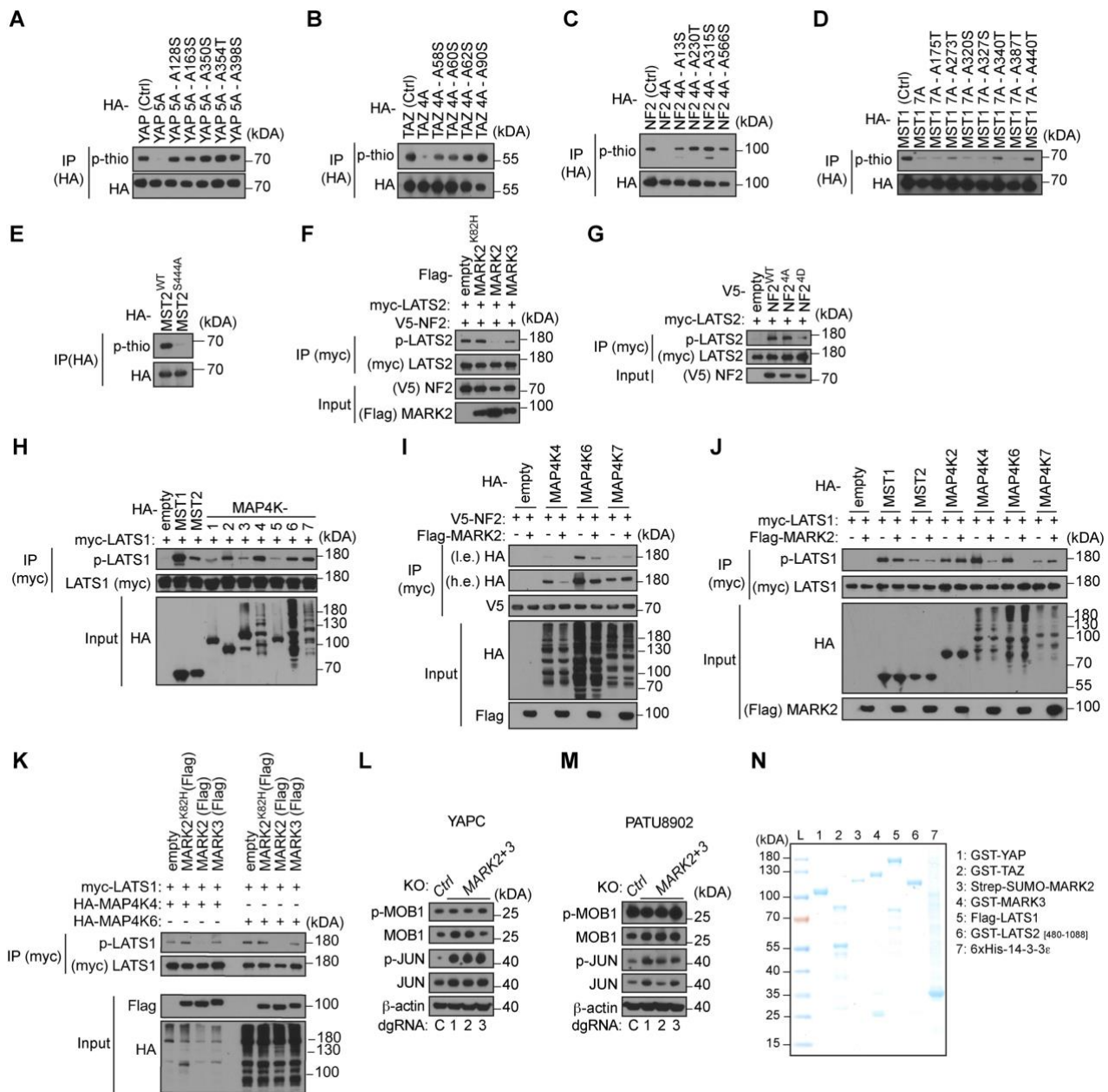


976
977
978
979
980
981
982
983

Supplementary Fig. S3.

A, Western blot analysis of Cas⁹+ YAPC cells. **B-D**, Western blot analysis of b,c MARK2 or d, MARK3 specific in-cell phosphorylation of Hippo pathway components. Substrates were labeled as described in **Fig. 3D**, and phosphorylation was identified by staining with thiophosphate ester-specific antibodies. Data are representative of two independent experiments. **E**, Coomassie stain of affinity purified recombinant Strep-SUMO tagged MARK2 (rMARK2) purified from insect cells. **F**, Western blot analysis of purified HA-CDC25C following treatment of Lambda phosphatase (λ -PP) and

984 phosphorylation using rMARK2. **g**, Lolli-pop illustration of MARK2-dependent phosphorylation sites
985 on MST1/2 and MAP4K1-4,6,7 identified using mass spectrometry-based phosphoproteomics.
986 SARAH= Sav/Rassf/Hpo domain, CNH= Citron homology domain.
987



993

994

Supplementary Fig. S5.

995

A-E, Western blot analysis of MARK2 specific substrates phosphorylation. Labeling as described in **Fig**

996

3d. Data are representative of two independent experiments. **F**, IP-western blot analysis evaluating the

997

phosphorylation p-LATS2 (T1041) in presence or absence of MARK2 or MARK3 following NF2

998

overexpression in HEK-293T cells. Data are representative of two independent experiments. **G**, IP-

999

western blot analysis evaluating the phosphorylation p-LATS2 (T1041) after NF2 mutant overexpression

1000

in HEK-293T cells. Data are representative of two independent experiments. **H**, IP-western blot analysis

1001

evaluating the phosphorylation p-LATS1 (T1079) following indicated gene overexpression in HEK-

1002

293T cells. **I**, IP-western blot analysis evaluating the interaction of NF2 and MAP4K4,6,7 in presence

1003

or absence of MARK2 overexpression in HEK-293T cells. Data are representative of two independent

1004

experiments. **J**, IP-western blot analysis evaluating the phosphorylation p-LATS1 (T1079) following

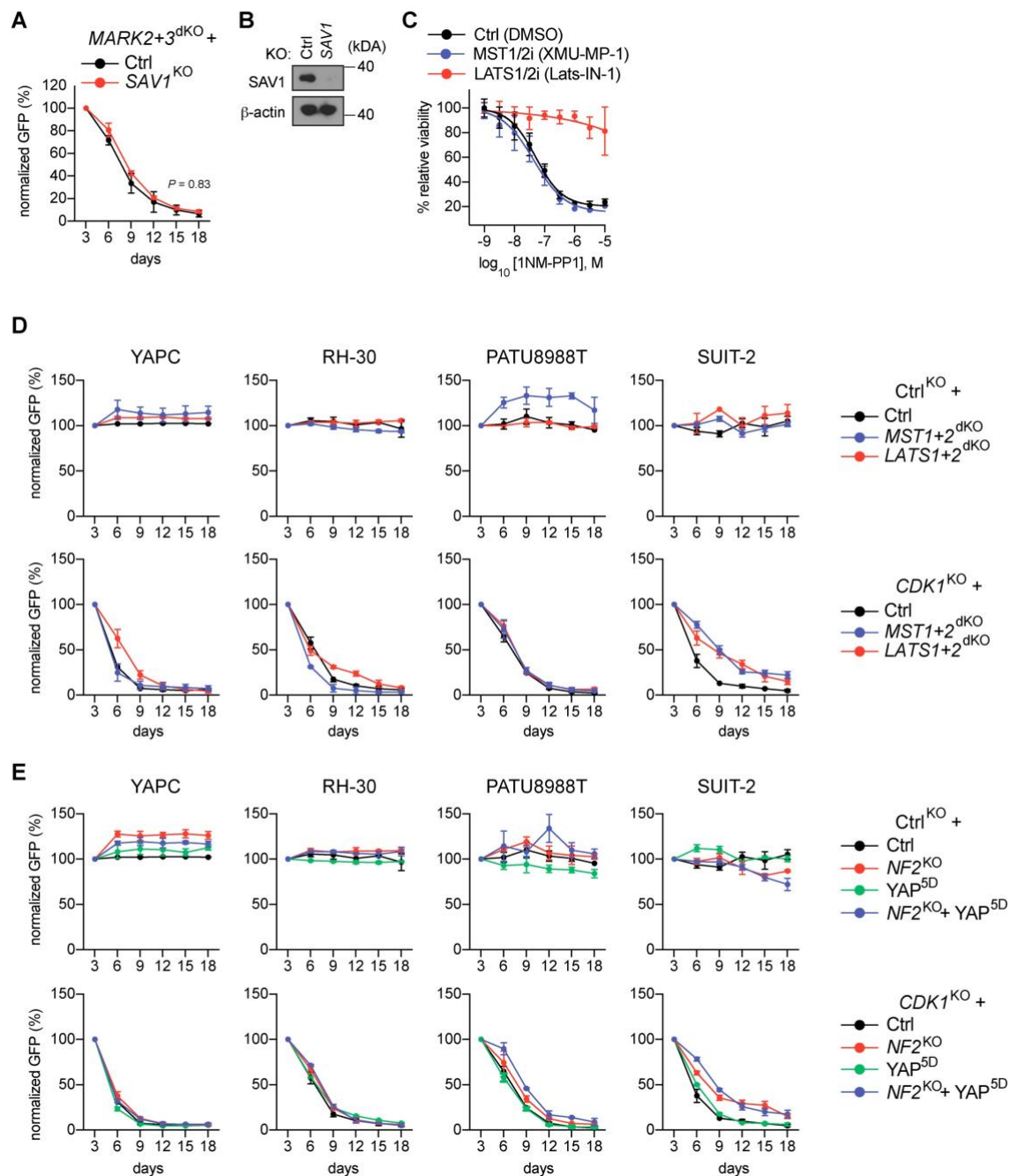
1005

indicated gene overexpression in HEK-293T cells. Data are representative of two independent

1006

experiments. **K**, IP-western blot analysis evaluating p-LATS1 (T1079) in presence of MAP4K4 or

1007 MAP4K6 together with MARK2,3, kinase dead MARK2^{K82H} or empty vector control overexpression in
1008 HEK-293T cells. Data are representative of two independent experiments. **L,M**, Western blot analysis
1009 of Cas9⁺ indicated cell lines. **N**, Coomassie stain of recombinant proteins used in *in vitro* kinase assays
1010 (**Fig.3K, 3L**), purified from bacteria (GST-YAP, GST-TAZ) and insect cells.

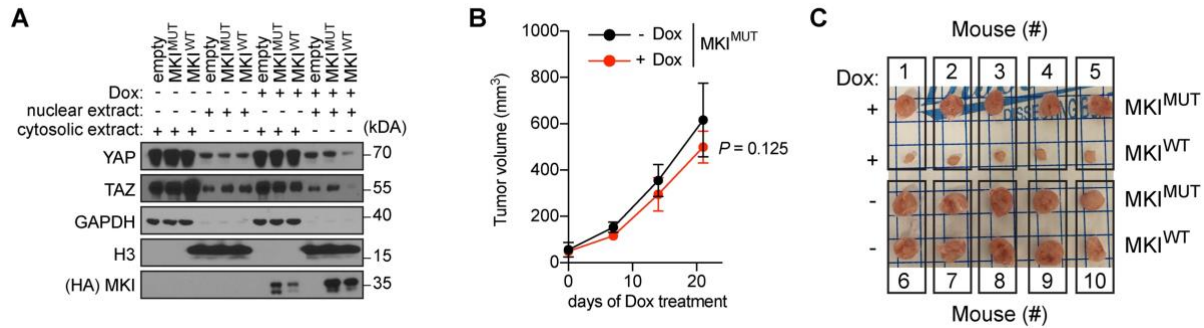


1011
 1012
 1013
 1014
 1015
 1016
 1017
 1018
 1019
 1020
 1021

Supplementary Fig. S6.

A, Rescue experiment of *MARK2+3^{dKO}* in Cas9⁺ YAPC cells following knockout of indicated genes. Data shown are the mean \pm SD of %GFP⁺ (normalized to day 3 after infection). $n=3-6$. P values are calculated using a mixed effects model (considering the interaction of experimental groups over time) compared to Ctrl group and corrected with Bonferroni-Holm (BH). **B**, Western blot analysis of YAPC cells. **C**, Normalized relative luminescence units (RLU) from CellTiter-Glo viability measurements of Cas9⁺ YAPC-*MARK2+3^{dKO}* + *MARK2^{M129G}* cells following 5 days of combinational treatment of 1NM-PP1 and either +DMSO (0.1%), +500nM MST1/2 inhibitor (XMU-MP-1) or + 5 μ M LATS1/2 inhibitor (Lats-IN-1). Data are shown as mean \pm SD. $n=9$ measurements from three biological replicates performed in triplicate. Four-parameter dose-response curves were plotted.

1022 **D,E** Competition-based fitness assays for Ctrl (dgRNA targeting hROSA26 locus) and knockout of
1023 essential gene *CDKI* corresponding to rescue experiment shown in **Fig. 4A, 4F**. Data shown are the
1024 mean \pm SD of %GFP⁺ (normalized to day 3 after infection). n=3-6.



1025

1026

Supplementary Fig. S7.

1027

1028

1029

1030

1031

1032

1033

1034

A, Western blot analysis of YAP localization following doxycycline (Dox) induced empty vector control, MKI^{WT} or MKI^{MUT} expression for 24h. Nuclear (Nuc) and cytosolic (Cyto) fractionation are indicated. (Data shown are an extension of **Fig. 5E**). **B**, Growth kinetics of subcutaneous YAPC xenografts implanted in immunodeficient mice. Expression of MKI^{MUT} from a Dox-inducible lentiviral construct was induced on day 10 post-injection of the cells. Data are shown as mean \pm SD $n=5$ per group. P values are calculated using a mixed effects model (considering the interaction of experimental groups over time) compared to Ctrl group (-Dox) and corrected with Bonferroni-Holm (BH). **C**, Tumor imaging at the end-point of the xenograft experiments shown in **B**, and **Fig. 5H**.

1035 **Contributions**

1036 O.K. and C.R.V. conceived this project and wrote the manuscript with input from all of the authors. O.K.
1037 and C.R.V. designed the experiments. O.K. performed experiments with help from D.S., C.T., A.A,
1038 F.M., D.A. and S.R.. O.K and T.H., performed statistical analysis. O.K. and O.E.D. designed CRISPR
1039 sgRNAs. O.K. designed and cloned paralog co-targeting CRISPR libraries. O.K. and D.S. screened
1040 libraries in cancer cell lines. O.K and C.T. performed experiments in subcutaneous xenografts. A.A.
1041 generated recombinant MARK2 proteins. F.M. and O.K. performed mass spectrometry sample
1042 preparations. F.M. and P.C. performed all mass spectrometry measurements. D.A., S.R. and O.K.
1043 performed organoid experiments. C.R.V., D.A.T., P.C., and D.L.S. supervised the studies and acquired
1044 funding.

1045

1046 **Competing interests**

1047 C.R.V. has received consulting fees from Flare Therapeutics, Roivant Sciences and C4 Therapeutics;
1048 has served on the advisory boards of KSQ Therapeutics, Syros Pharmaceuticals and Treeline
1049 Biosciences; has received research funding from Boehringer-Ingelheim and Treeline Biosciences; and
1050 owns a stock option from Treeline Biosciences. D.A.T. is a member of the Scientific Advisory Board
1051 and receives stock options from Leap Therapeutics, Surface Oncology, and Cygnal Therapeutics and
1052 Mestag Therapeutics outside the submitted work. D.A.T. is the scientific co-founder of Mestag
1053 Therapeutics. D.A.T. has received research grant support from Fibrogen, Mestag, and ONO
1054 Therapeutics. D.L.S. is a member of the Scientific Advisory Board of Flamingo Therapeutics and
1055 Amaroq Therapeutics. None of this work is related to the publication.